NATIONAL AERONAUTICS AND SPACE ADMINISTRATION
Washington, D. C.

NASA Grant NGL 44-012-006

PLANETARY OBSERVATIONS AT MILLIMETER WAVELENGTHS

B. L. Ulich
J. R. Cogdell
J. H. Davis

Technical Report No. NGL-006-72-1
31 January 1972

Submitted by

Electrical Engineering Research Laboratory
The University of Texas at Austin
Austin, Texas

NATIONAL AERONAUTICS AND SPACE ADMINISTRATION
Washington, D. C.

NASA Grant NGL 44-012-006

PLANETARY OBSERVATIONS AT MILLIMETER WAVELENGTHS

B. L. Ulich
J. R. Cogdell
J. H. Davis

Technical Report No. NGL-006-72-1
31 January 1972

Submitted by

Electrical Engineering Research Laboratory
The University of Texas at Austin
Austin, Texas

ABSTRACT

Observations of the Sun, Moon, Mercury, Venus, Mars, Jupiter, and Saturn were made at 3.1 mm and 8.6 mm wavelengths with the 16 foot radio telescope at the Millimeter Wave Observatory between March and August, 1971. The measured absolute brightness temperatures are tabulated below.

SUMMARY OF RESULTS

Source	Wavelength (mm)	Temperature (°K)	Accuracy, 1σ(°K)	Notes
Sun	3.1	6573	218	Disk average
Sun	8.6	7280	245	Disk average
Moon	3.1	215	6	Center of Moon, averaged over a lunation
Mercury	3.1	373 + 169 cos (φ+18°)	35	
Venus	2.14	564	100	Preliminary measurement
Venus	3.1	386	33	φ = 300°
Venus	8.6	503	102	φ = 300°
Mars	3.1	217	16	
Mars	8.6	224	38	
Jupiter	3.1	185	13	
Jupiter	8.6	174	20	
Saturn	3.1	151	11	
Saturn	8.6	102	24	

All errors are one standard deviation and include uncertainties in antenna gain calibration. The solar and lunar temperatures are in excellent agreement with published observations. The planetary measurements at 3.1 mm

are consistently higher than previous results. The implications of higher temperatures with respect to existing atmospheric and surface models are discussed.

Although we have only observed a portion of the phase variation of the brightness temperature of Mercury, the per cent phase variation and phase lag we derive are consistent with previous results at similar wavelengths. The higher mean temperature of about 375°K, however, indicates that the spectrum is flat between 3 mm and 6 cm wavelength. Thus the thermal conductivity of the Mercurian epilith appears to be independent of temperature.

Our measurements of Venus, which also indicate higher temperatures than expected, reveal that published model calculations of the spectrum of Venus have not treated the induced absorption of CO_2 correctly, and that perhaps more laboratory measurements of CO_2 absorption are needed in the millimeter region. With this correction our results are only marginally consistent with assumed constant mixing ratios of CO_2, and argue weakly for there being little H_2O and O_2 at the 300°K to 400°K level in the Venusian atmosphere where the 3 mm emission originates.

The spectrum of Mars was confused because of inaccurate absolute measurements of Mars and Jupiter at millimeter wavelengths. Our more accurate measurements of Jupiter have removed much the scatter in the spectrum of Mars since more than half the Mars millimeter observations were made relative to Jupiter. The spectrum does turn up at shorter wavelengths, and, within the accuracy of the measurements, is fit by

the homogeneous thermal model with material properties similar to those of the Moon. The presence of a thin layer of liquid water is highly unlikely.

Our value of 185±13°K for the brightness temperature of Jupiter at 3.1 mm wavelength indicates a more transparent window between the ammonia and hydrogen absorption lines than expected. The measurements are not in good agreement with published models, which are based on a lower effective temperature than that measured by Aumann et al. (1969). Until further model calculations are made, no conclusions can be drawn regarding the distribution of NH_3 in the atmosphere.

Our observations of Saturn are consistent with thermal emission from a deep atmosphere with a large temperature gradient and an opacity which depends on wavelength. The brightness temperature at millimeter wavelengths is about 150°K.

TABLE OF CONTENTS

		Page
I.	Introduction	1
II.	Equipment	2
	A. Antenna	2
	B. Receivers	3
	C. Data Recording and Handling	8
III.	Observations	9
	A. Ephemerides	9
	B. Observing Procedure	9
	1. Sun	9
	2. Moon	9
	3. Planets	11
IV.	Results	12
	A. Sun and Extinction Data	12
	B. Moon	16
	C. Planets	16
	1. Mercury	19
	2. Venus	20
	3. Mars	22
	4. Jupiter	23
	5. Saturn	24
V.	Discussion of Results	25

A. General Considerations 25

B. Planetary Spectra 30

1. Jupiter 30

2. Mercury 39

3. Venus 44

4. Mars 48

5. Saturn 57

Appendix 62

A. Data Analysis 62

1. Data Recording 62

2. Extinction Data 62

3. Lunar Data 63

4. Planetary Data 67

B. Error Analysis 72

1. General Considerations 72

2. Antenna Temperature 76

3. Peak Antenna Temperature 78

4. Brightness Temperature 79

5. Summary 81

References 82

LIST OF FIGURES

No.		Page
1	Receiver Block Diagram	4
2	Typical Solar Drift Scan	10
3	3.1 mm Average Solar Disk Temperature	13
4	8.6 mm Average Solar Disk Temperature	14
5	3.1 mm Average Solar Disk Temperature - Selected Data	15
6	Variation of 3.1 mm Extinction with Absolute Humidity	17
7	3.1 mm Lunation Curve	18
8	3.1 mm Mercury Data	21
9	Spectrum of Jupiter above 15 GHz	31
10	16 Foot Antenna Efficiency Diagram	36
11	Mean Disk Temperature of Mercury	41
12	Microwave Spectrum of Venus	45
13	Mars Radio Spectrum	52
14	Microwave Spectrum of Saturn	59
A1	3.1 mm Extinction Data	64
A2	3.1 mm Flux Enhancement	65
A3	3.1 mm Variable Extinction	66
A4	Bias of Least Squares Fit	70

LIST OF TABLES

No.		Page
I	Millimeter Wave Observatory 16 Foot Antenna Parameters	3
II	3.1 mm Noise Tube Calibrations	7
III	8.6 mm Noise Tube Calibrations	7
IV	Mercury Observations	20
V	Venus Observations	22
VI	Mars Observations	23
VII	Jupiter Observations	24
VIII	Saturn Observations	25
IX	Comparison of the 3 mm Planetary Brightness Temperatures Reported Here With Those of Epstein *et al.*	27
X	Reported Mean Temperatures of Mercury	42
XI	Radio Observations of Mars	49
XII	Radio Observations of Saturn	58
AI	Error Summary	81

I. INTRODUCTION

The purpose of this report is to describe in some detail the techniques and procedures in current use in the program of planetary observations, and to report the results of these observations to the present time. In Section II we describe the major equipment used in the program. The antenna has been dealt with in three previous reports (Cogdell, 1969a, Davis and Cogdell, 1969, and Davis, 1970) and is not treated in depth here. More emphasis is placed rather on receiver operation and calibration, as well as on data recording and handling procedures. In Section III we describe the way in which the planetary observations are made. This includes details of how the observing ephemeris is prepared as well as a description of the observing routine by which the data are generated. In Section IV the results of the measurements are presented. The program is ongoing so this section serves as a status report as of the time of writing. In Section V the results are discussed in relation to other measurements and planetary models. In the Appendix data analysis is discussed. There we show how the atmospheric attenuation is determined. The major part of the section presents the procedures through which the raw data generated during the observation are converted to an estimate of the disk temperature of the planet for that day. The appendix also contains the error analysis of the measurements. We discuss the biasing errors of calibation as well as various effects introduced in the data analysis procedures.

II. EQUIPMENT

A. Antenna

The antenna used in the measurements is a paraboloid 4.88 meters (16 feet) in diameter. The antenna was originally located at The University of Texas Balcones Research Center, Austin, Texas in 1963. Its performance was reported by Tolbert et al. (1965) and it was used at this site for planetary measurements (Tolbert and Straiton, 1964, and Tolbert, 1966) as well as for measurements of the Sun (Takahashi, 1967), Moon (Clardy and Straiton, 1968) and galactic objects (Tolbert, 1965, and Tolbert and Straiton, 1965).

In 1967 the antenna was refurbished and moved to Mt. Locke, Texas, 450 miles west of Austin. The purpose of this move was to benefit from the superior climate resulting from the high elevation (2070 meters) and general dryness of the area.

The move of the antenna necessitated a complete recalibration. This work is described in detail by Cogdell (1969a), Davis and Cogdell (1969), and Davis (1970). A summary of the antenna properties is given by Cogdell et al. (1970). The techniques relating to the gain measurement were developed by Davis and Cogdell (1971). Some of the work pertaining to the pointing calibration appears in Davis and Cogdell (1970). Some astronomical measurement are reported in Ulich (1972) and Cogdell (1972).

For the present work the only relevant antenna properties are the patterns and peak gains at f = 97.1 GHz (λ = 3.1 mm) and f = 35.0 GHz (λ = 8.6 mm). These properties are summarized in Table I.

TABLE I

MILLIMETER WAVE OBSERVATORY
16 FOOT ANTENNA PARAMETERS

Frequency (GHz)	Wavelength (mm)	Efficiency (%)	3 dB Beamwidth (°)	Sidelobe Level (dB)
35.0	8.6	67.2±0.9(1σ)	.110	-24
97.1	3.1	53.7±2.8(1σ)	.042	-21

B. Receivers

The receivers used in the planetary program are superheterodyne Dicke radiometers. The receiver consists of a balanced mixer followed by IF amplifiers having a passband from 100-200 MHz and approximately 90 dB gain. Square law detection is accomplished in a semiconductor diode and lock-in amplification in a commercial amplifier-detector. The receiver is switched synchronously between the antenna feed horn and a reference sky horn by a switchable four-port ferrite circulator. The calibration signal is derived from a neon discharge noise tube and is injected into the reference port by means of 20 dB directional coupler. Hence the calibration signal appears as a negative deflection at the output. An attenuator is placed between the noise tube and the directional coupler for the purpose of reducing the calibration signal should that be required. In the case of the 8.6 mm radiometer, an isolator is used between the four-port switchable circulator and the mixer to reduce the effect of klystron noise. A block diagram of the receiver is shown in Fig. 1. The performance of the

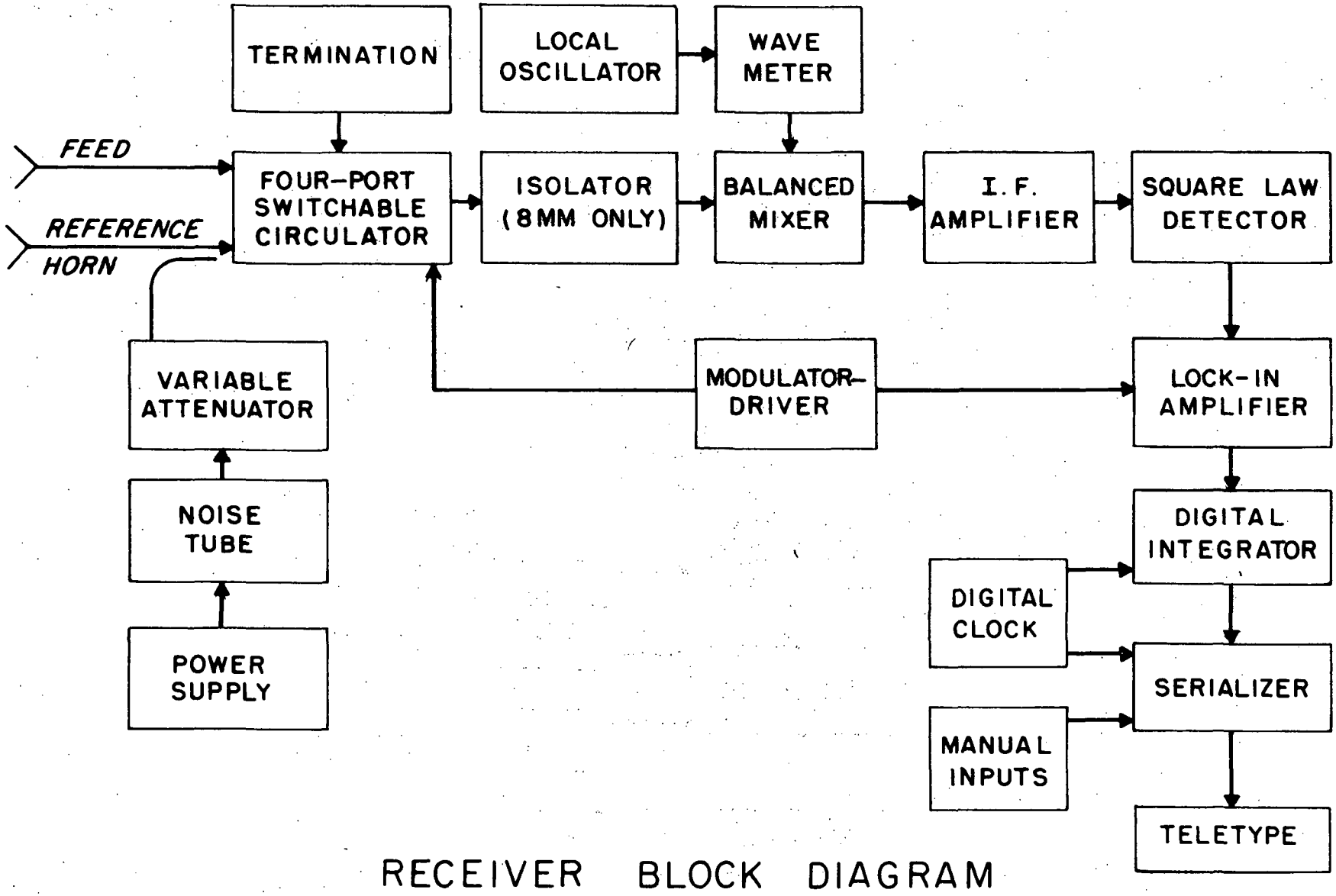

RECEIVER BLOCK DIAGRAM

Fig. 1

receivers depends on the system temperature (T_s), bandwidth (B), and integration time (t) according to the formula

$$\Delta T_{rms} = \frac{K_s T_s}{\sqrt{Bt}} \qquad (1)$$

where ΔT_{rms} is the standard deviation of the output data in equivalent thermal units at the input, and $K_s = 2.22$ for the modulation-detection scheme used in the receivers. In the course of the observations, the sensitivity (ΔT_{rms} for t = 1 sec) is automatically monitored through the calibration procedure. Typical values are 2°K for the 8.6 mm system and 3 to 5°K for the 3mm system. The latter varies according to the health of the local oscillator klystron, since the noise generated in the klystron and self-mixed into the IF bandpass makes a significant contribution to the system temperature. The performance of the receivers is the limiting factor in the accuracy and scope of the planetary measurements program at the present time, and our efforts are currently being concentrated toward improving their sensitivity.

One purpose of the planetary measurements program is to make absolute measurements of the flux from those planets which we can detect. Most models of planetary atmospheres and surfaces require such absolute (as opposed to relative) measurements. In addition, some planets, principally Jupiter, are used as primary calibration sources for millimeter radio telescopes which cannot be calibrated by other means, and hence the flux scale for many millimeter observations depends on an accurate

knowledge of the temperatures of these planets. For these reasons, the calibration of the receivers is of great importance to the program. The calibration signals originate in neon noise tubes and are coupled into the reference port of the ferrite modulator by a directional coupler. When the noise tubes are fired, the effect is to indicate a decrease in the antenna temperature by a constant amount. This calibration signal is evaluated in thermal units (°K) of antenna temperature and referred to the receiver input flange by direct comparison with a well-matched termination immersed in boiling water and ice slush. Corrections are made for the estimated VSWR of the termination and loss between the termination and the receiver input flange. Since the gain of the antenna is also referred to the receiver input flange, our referencing of the calibration signal to the same point in the system allows direct inference of antenna temperature without further corrections.

The same calibration signal has been used at 3.1 mm since the beginning of the program. This signal has been thermally calibrated a number of times with reasonably consistent results in spite of the fact that the waveguide assembly was disassembled several times during this period. The various evaluations of the 3.1 mm calibration are tabulated in Table II. Clearly there are too few samples to give firm meaning to the quoted standard deviation, but the impression given is one of good repeatability.

TABLE II

3.1 MM NOISE TUBE CALIBRATIONS

Date	Calibration Signal (°K)
December 8, 1969	81.7
April 18, 1971	84.3
June 1, 1971	78.6
August 12, 1971	79.3
August 17, 1971	83.4
Average	81.4±1.3°K(1σ)

At 8.6 mm two different calibration signals were used during different periods of observations. Multiple thermal calibrations of these signals were not attempted, so no estimate of internal accuracy can be made. Our experience, however, indicates that the 8.6 mm equipment is generally better behaved than the 3.1 mm equipment, so we would expect equivalent or better repeatability at the longer wavelength than at the shorter. The 8.6 mm calibrations are given in Table III.

TABLE III

8.6 MM NOISE TUBE CALIBRATIONS

Period	Calibration Signal (°K)
Prior to August 12, 1971	436
After August 12, 1971	39.0

The derived calibration signal value is put into the data reduction program, where the data are automatically corrected for receiver gain variation during an observing run and calibrated in terms of antenna temperature.

C. Data Recording and Handling

As detailed in the next section, during an observing period the radio telescope is sequenced through a number of operations, namely, solar scans, baseline, source, and calibrations. Each of these "scans" is composed of a sequence of data groups. These groups are of two kinds: the first and last contain information such as time, antenna position, function being performed, integration time per point, and the like; in between are a sequence of data points which are the receiver output integrated over consecutive periods of time.

Let us follow the receiver output signal through the data handling process. The output of the second (square law) detector is amplified and synchronously detected in the lock-in amplifier and smoothed with a single pole RC low pass filter. The output of the lock-in amplifier is then applied to an integrating voltmeter, which integrates for a preset period of time (usually 2, 4, or 10 seconds) and then delivers the data to a serializer in BCD form. The serializer converts to ASC III, 8 level code and feeds the data to a teletype for a punched paper tape and hard copy. Any known errors in the data, such as an incorrect antenna position, are recorded in a log book.

At the end of the observing run, the tape, hard copy, and error log are sent to Austin. The tapes are translated and recorded on magnetic

tape. The data are then rerun on a CDC 6600 computer and translated to Hollerith code, grouped into records corresponding to the teletype hard copy lines, and punched on cards. After the cards are interpreted and known errors are edited, the data are ready for analysis in our various radio astronomy data reduction programs.

III. OBSERVATIONS

A. Ephemerides

Ephemerides were prepared on a digital computer prior to actual observations. Geocentric positions at epoch 1950.0 were obtained from Jet Propulsion Laboratory magnetic tape DE69. These positions were corrected for precession, nutation, aberration, and topocentricity. Corrections for mount eccentricities (Davis and Cogdell, 1969), encoder offsets, sag, and refraction (Davis and Cogdell, 1970) were then applied to produce servo readings for solar system objects as a function of local time.

B. Observing Procedure

1. Sun

Solar observations were made to calculate the attenuation of the earth's atmosphere. Drift scans were taken through the center of the disk over a wide range of zenith angle. Figure 2 shows a typical drift scan taken at 3.1 mm. Data were taken for several hours after sunrise, for about an hour at noon, and again for several hours before sunset.

2. Moon

The 3.1 mm brightness temperatures of several regions near the Moon's mean center were monitored during an entire lunation.

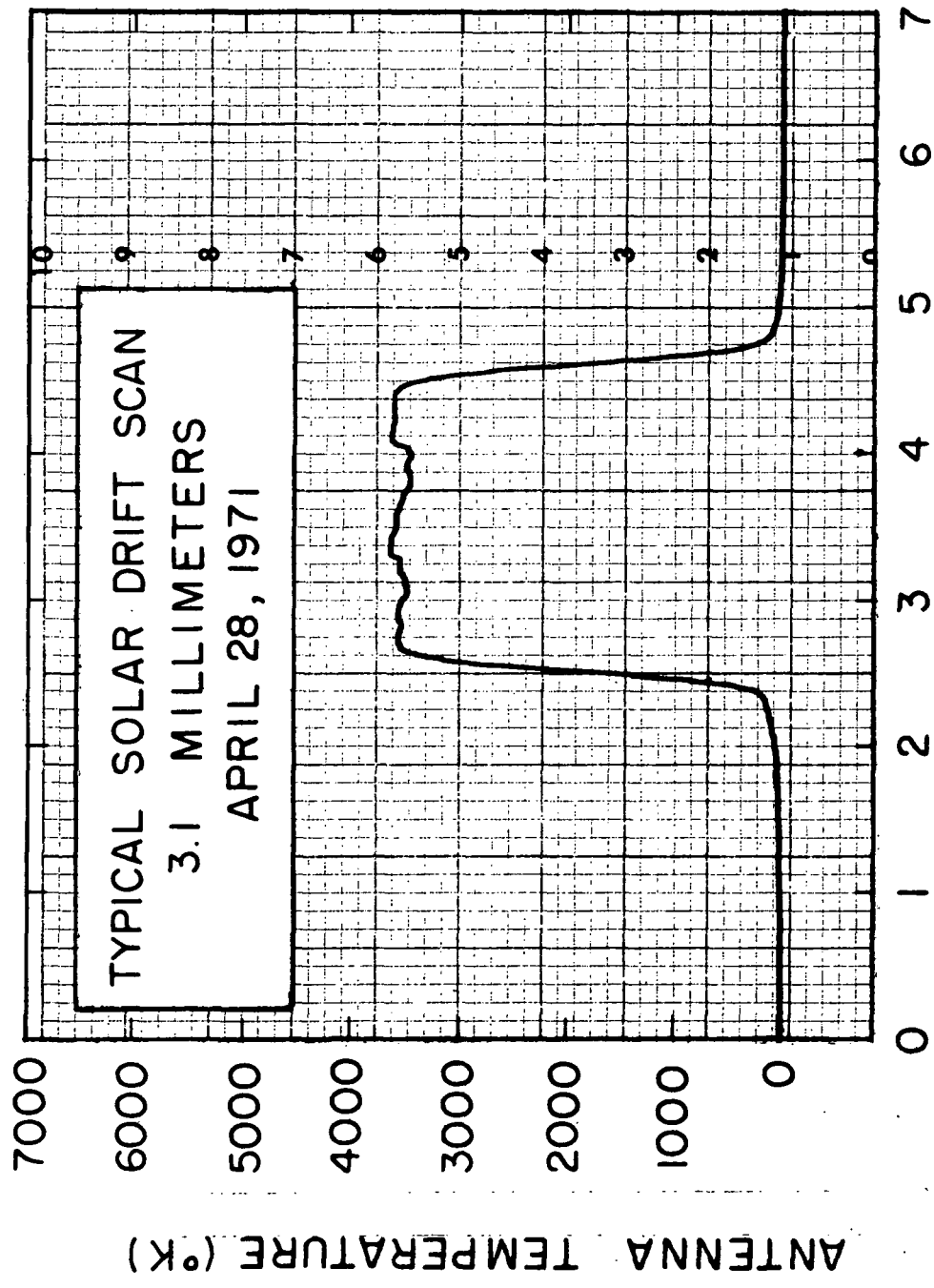
TYPICAL SOLAR DRIFT SCAN
3.1 MILLIMETERS
APRIL 28, 1971
ANTENNA TEMPERATURE (°K)
7000
6000
5000
4000
3000
2000
1000
0
0
1
2
3
4
5
6
7
TIME (MINUTES)

Fig. 2

The results will be reported elsewhere. The average value observed can serve as a check of the thermal calibration, as this value is almost independent of wavelength according to Krotikov and Troitskii (1964). In these observations the standard ON-OFF method of observation was used.

3. Planets

Planetary observations were made using a modified OFF-ON-OFF technique. Blank sky was observed before and after the planet was observed. During these blank sky baseline scans the antenna was driven across the sky along the same path as the planet took. Thus stray back-lobe pickup and atmospheric emission were effectively cancelled. In addition the uncertainty of the measurement was minimized by spending half of the baseline integration time on each side of the source integration.

Jupiter and Venus were observed at the predicted planetary positions and also at the four cardinal points one-half the HPBW away. Because of their relatively weak signals, Mercury, Mars, and Saturn were only observed at the predicted ephemeris position. In this manner sufficient integration time for a reasonable measurement was accumulated during a single observing period. Since the point source response of the antenna is known from pattern range measurements, knowledge of the pointing error relative to the ephemeris enables one to correct the observed signal strengths to the values one would measure with perfect pointing. All planetary observations were made within four hours of transit to minimize atmospheric extinction losses.

Calibration of the receiver was accomplished by periodically injecting a signal of known equivalent temperature from a gas discharge tube. This allows one to correct for changes in receiver gain and to calibrate the output deflection in terms of antenna temperature.

IV. RESULTS

A. Sun and Extinction Data

Drift scans were taken of the Sun on 62 days at 3.1 mm and on 9 days at 8.6 mm. Plots of the average brightness temperature across the center of the disk versus zenith attenuation are shown in Fig. 3 and 4. The thermal calibration used was the same as in the planetary measurements. The video amplifier gain was reduced to keep the signal on scale, thus adding 1% uncertainty in these values. The lack of slope of a least squares fit of a straight line to the data indicates that the Sun's apparent temperature is uncorrelated with the measured atmospheric extinction. Average solar temperatures were found to be 6440±223°K at 3.1 mm and 7280±245°K at 8.6 mm. A more accurate estimate of the solar temperature at 3.1 mm was obtained by selecting data on the basis of a good linear fit of the extinction plot. Scatter due to temporal variations in the attenuation and the solar flux was considerably reduced. Figure 5 shows that the 3.1 mm selected data yields an estimated solar disk temperature of 6573±218°K, in excellent agreement with the 3.3 mm temperature of 6567±152°K reported by Reber (1970). This value is consistent with the Van de Hulst model fit to existing measurements by Shimabukuro and Stacey (1968).

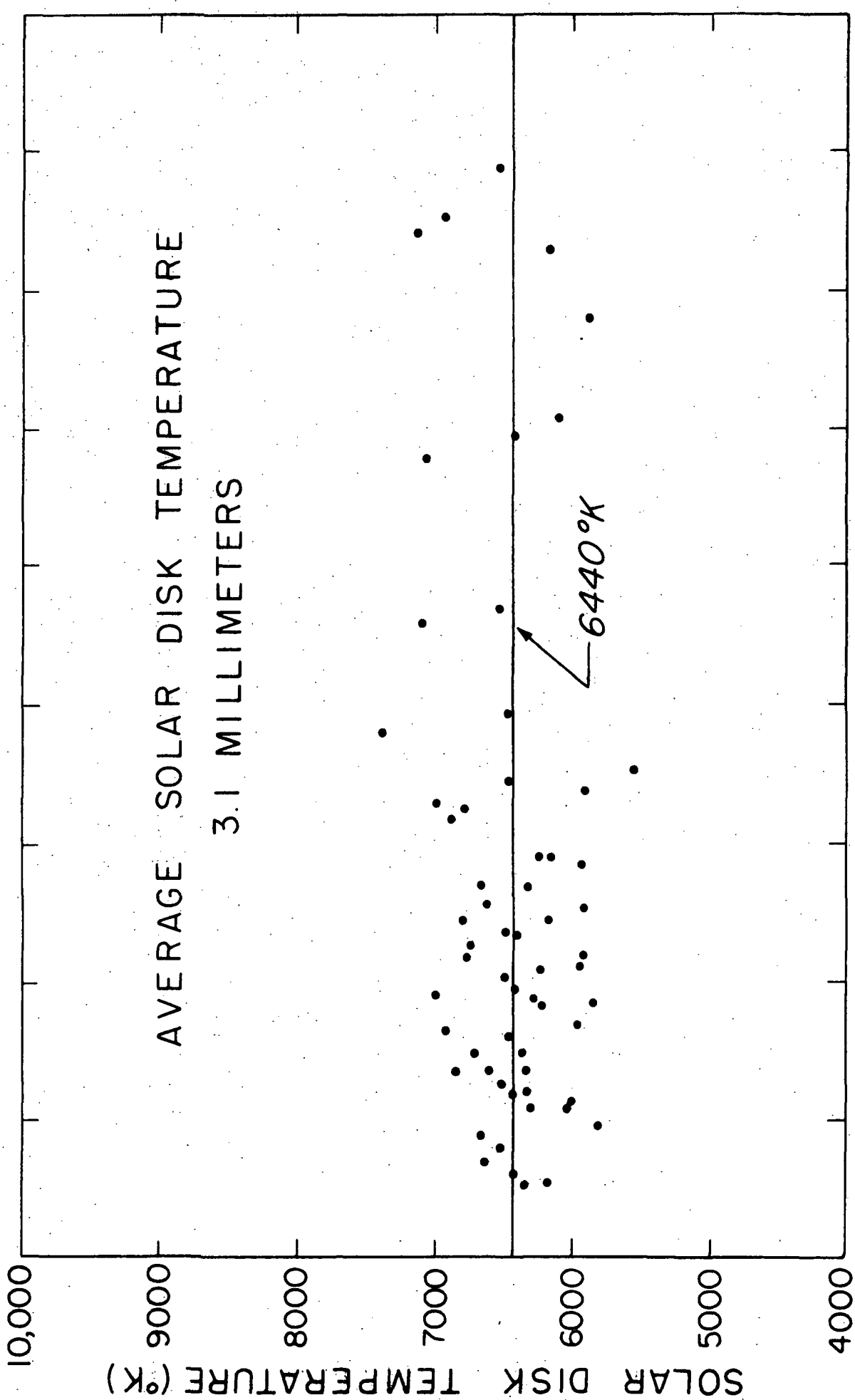
AVERAGE SOLAR DISK TEMPERATURE
3.1 MILLIMETERS
6440°K
SOLAR DISK TEMPERATURE (°K)
10,000
9000
8000
7000
6000
5000
4000
0
.1
.2
.3
.4
.5
.6
.7
.8
.9
ZENITH ATTENUATION (dB)

Fig. 3

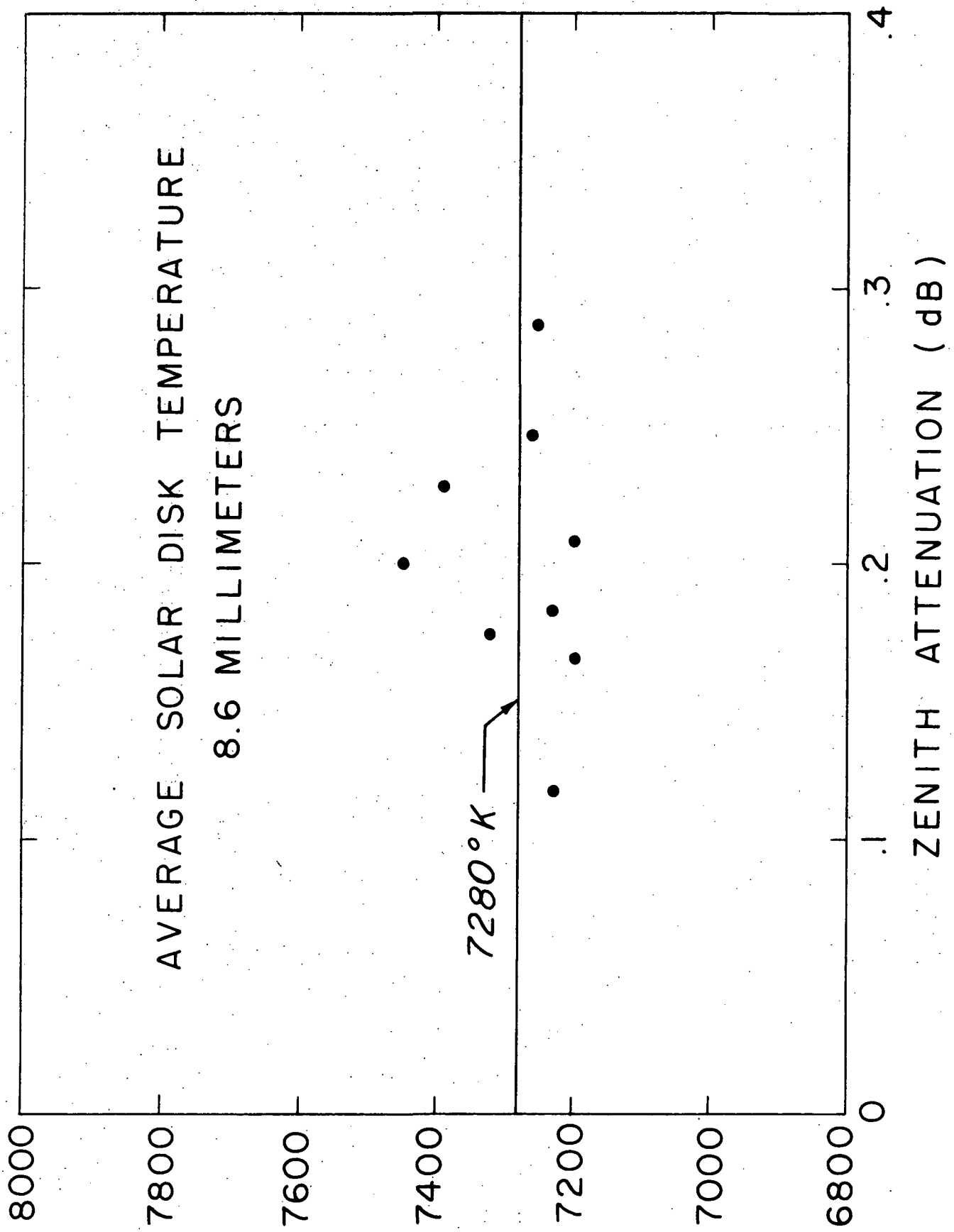
AVERAGE SOLAR DISK TEMPERATURE
8.6 MILLIMETERS
7280° K
SOLAR DISK TEMPERATURE (°K)
8000
7800
7600
7400
7200
7000
6800
0
.1
.2
.3
.4
ZENITH ATTENUATION (dB)

Fig. 4

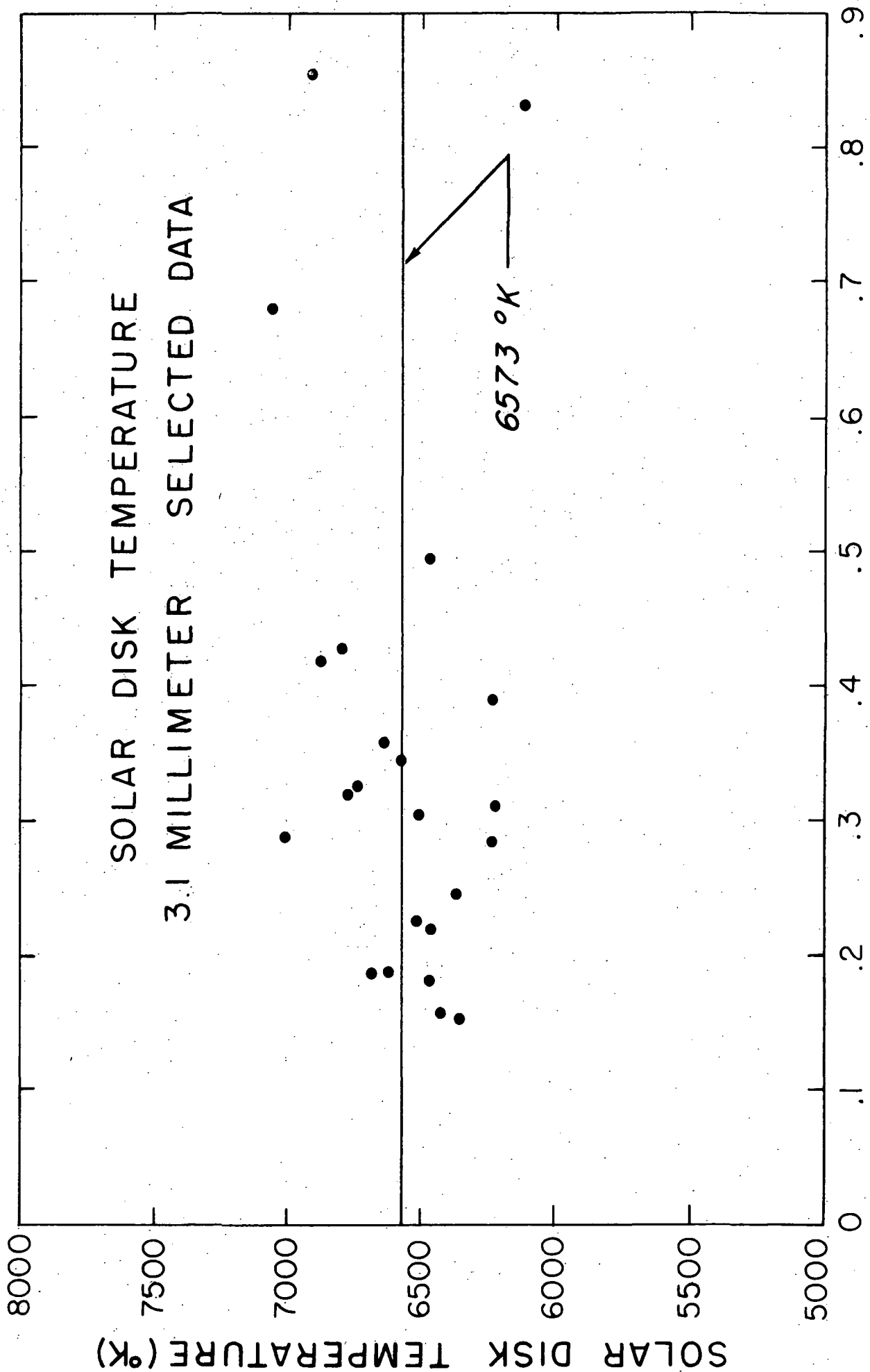
SOLAR DISK TEMPERATURE
3.1 MILLIMETER SELECTED DATA
6573 °K
SOLAR DISK TEMPERATURE (°K)
8000
7500
7000
6500
6000
5500
5000
0
.1
.2
.3
.4
.5
.6
.7
.8
.9
ZENITH ATTENUATION (dB)

Fig. 5

Psychrometric data taken during some of the solar observations were used to calculate the surface absolute humidity. Figure 6 is a plot of zenith attenuation versus absolute humidity at 3.1 mm. It is evident that there is considerable correlation. The scatter in the data is probably due to the fact that the attenuation measurements represent an average over a period of several hours, while the surface absolute humidity was only measured once during the observing period. The line fit to the data is represented by the equation

$$\alpha = .10 + .09\,\rho \qquad (2)$$

where

α = Zenith attenuation (dB)

ρ = Surface absolute humidity (g/m^3)

This method allows one to quickly estimate the extinction at any time by measuring the absolute humidity at the observing site.

B. Moon

The mean brightness temperature of the center of the moon averaged over a lunation can be used as a calibration source. As shown in Fig. 7 the value obtained at 3.1 mm is 215±6°K. This result is consistent with the value of 213±24°K derived by Low and Davidson (1965) at 1 mm and the value of 207±2°K at centimeter wavelengths as determined by Troitskii (1967).

C. Planets

In this section we tabulate the planetary measurements on a daily basis. In the tables we give the wavelength, date, measured brightness

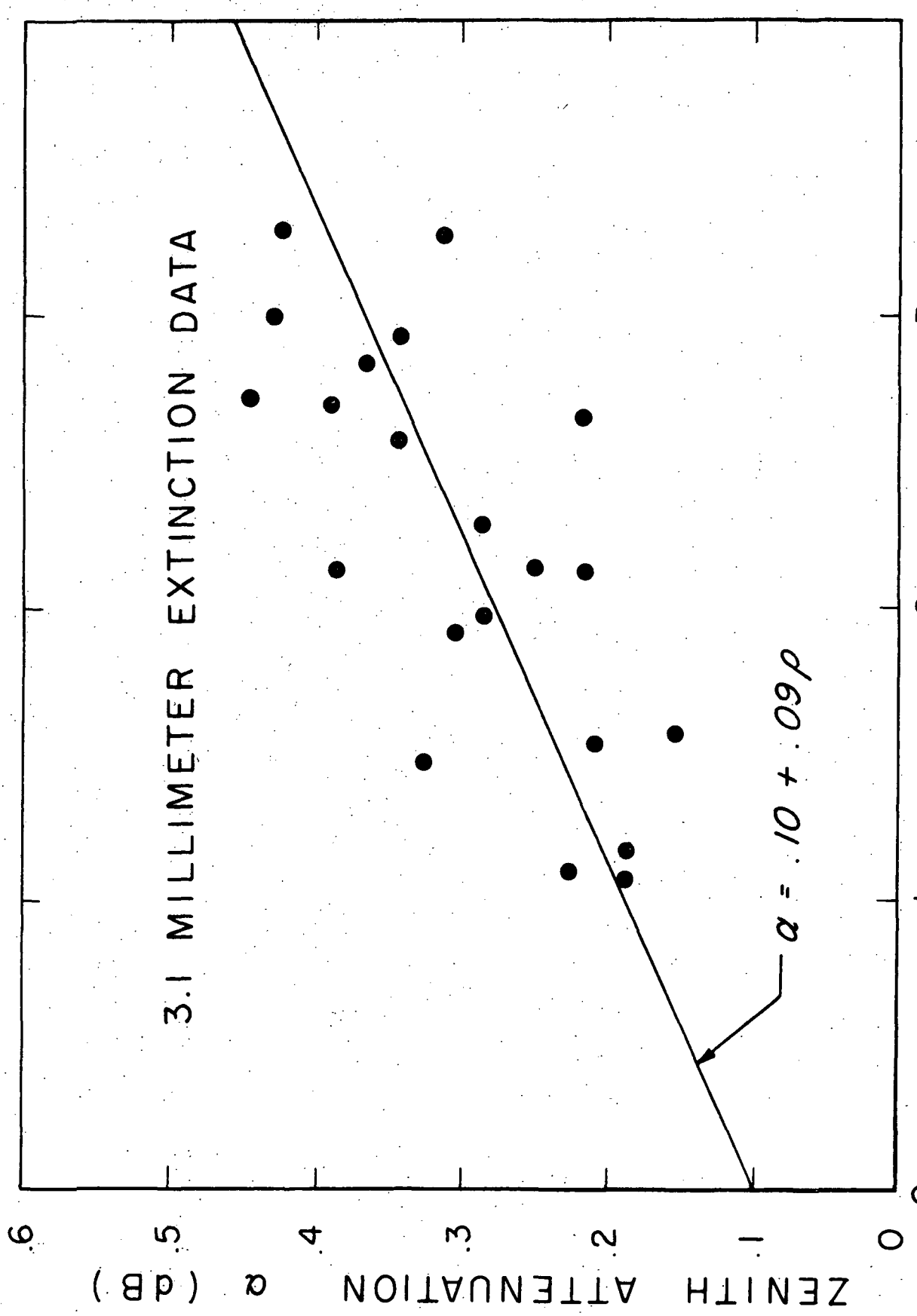
3.1 MILLIMETER EXTINCTION DATA
$\alpha = .10 + .09\rho$
ZENITH ATTENUATION α (dB)
ABSOLUTE HUMIDITY ρ (g/m^3)
0
1
2
3
4
.6
.5
.4
.3
.2
.1
0

Fig. 6

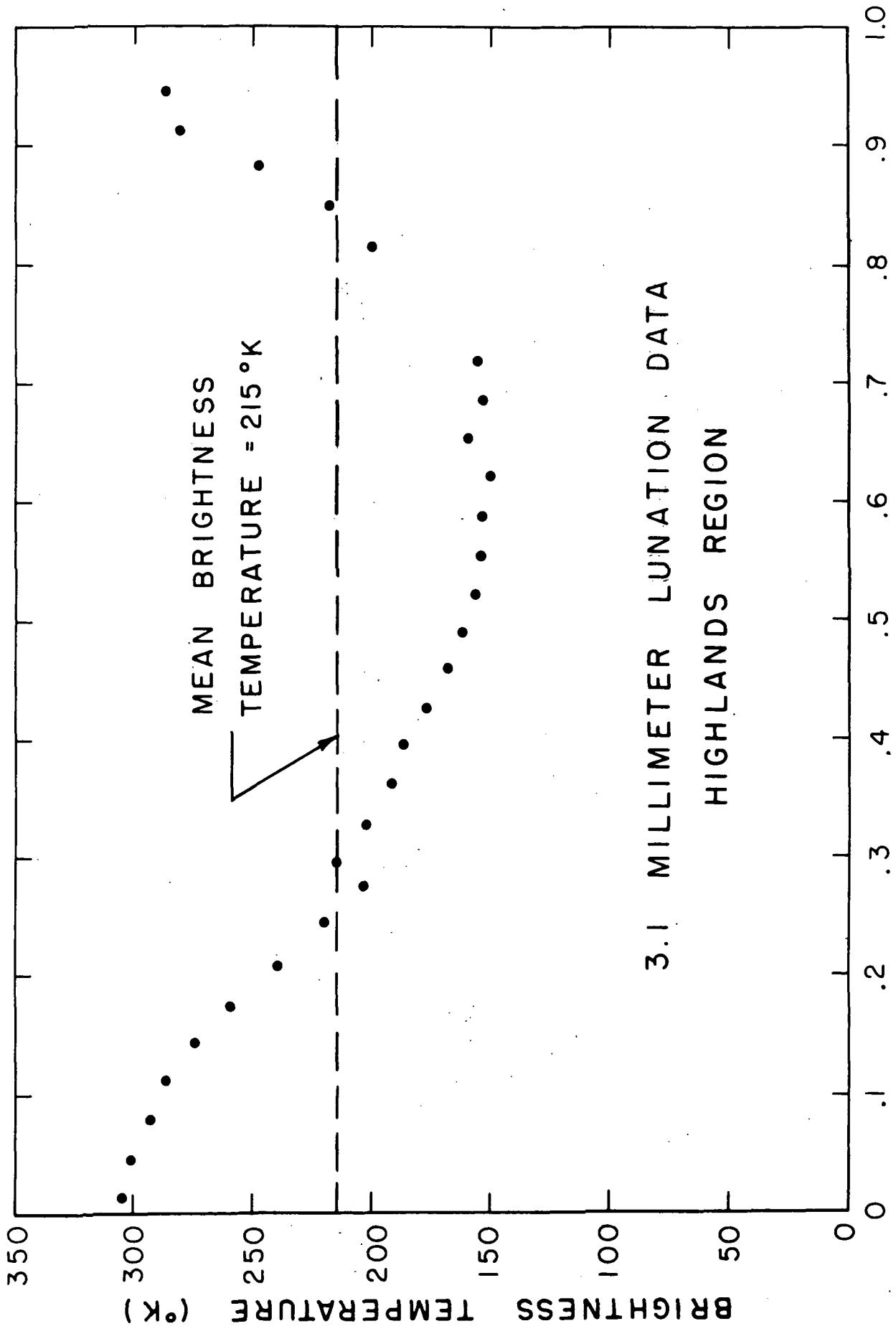
BRIGHTNESS TEMPERATURE (°K)
350
300
250
200
150
100
50
0
0
.1
.2
.3
.4
.5
.6
.7
.8
.9
1.0
FRACTION OF PERIOD
3.1 MILLIMETER LUNATION DATA
HIGHLANDS REGION
MEAN BRIGHTNESS
TEMPERATURE = 215°K

Fig. 7

temperature, receiver noise, zenith attenuation, and method of observation (one point or five points). The accuracy of the daily values is estimated on the basis of integration time and receiver sensitivity as indicated by the calibrations, as explained earlier in this report.

In the case of Mercury, the data are fit to the expected phase curve. For the other planets, where no phase effects are expected, the data are averaged together, weighted inversely with variance. The accuracy of the average is estimated by two methods. The first comes from the daily accuracies and the weighting factors. The second is a statistic of the data. We compute the corrected standard error as

$$\sigma = \left(\frac{\sum_{i=1}^{N} T_i^2}{N(N-1)} - \frac{\left(\sum_{i=1}^{N} T_i \right)^2}{N^2(N-1)} \right)^{1/2} \times F_N \qquad (3)$$

where σ = Corrected standard error (°K)

T_i = Daily temperature values (°K)

N = Number of daily values used

F_N = Small sample correction factor

The factor F_N is the 68% confidence value for a student's t distribution for N-1 degrees of freedom divided by the 68% confidence value for a Gaussian distribution; typically $F_N \approx 1.1$. Hence our 1σ errors are to be interpreted as 68% confidence levels. In quoting errors, we conservatively chose the larger of the two estimates.

1. Mercury

Mercury was observed on 9 separate days, but in some cases

several days were averaged together because of the weak signal level. The data are given below in Table IV.

TABLE IV

MERCURY OBSERVATIONS

Wavelength (mm)	Date (1971)	T_B(°K)	σ_{T_B} (°K)	Φ(°)	α(dB)	Method
3.1	8/24	203	45	168	.855	1
3.1	8/26	224	52	192	.711	1
3.1	1/1, 8/30	246	38	200	.272, .992	1
3.1	5/1, 5/2	278	38	220	.300	1
3.1	5/13, 5/14, 5/15	368	40	250	.370, .482, .367	1

Because of the relatively poor receiver sensitivity, it was possible to make meaningful observations only near inferior conjunction, when the signal-to-noise ratio is greatest. Fitting a phase curve to data over a limited range in phase angle can lead to large errors. However, for discussion purposes, a least-squares fit of an equation of the form $T_0 + T_1 \cos(\Phi + \delta)$ was made to the data. The resulting fit of $T_B = 373 + 169 \cos(\Phi + 18°)$ is superimposed on the data in Fig. 8. It is felt that the apparently good fit to the observed values must be somewhat fortuitous in view of the probable measurement errors.

2. Venus

The data on Venus were taken during a short period in later March and early April. Data taken during midsummer were taken through

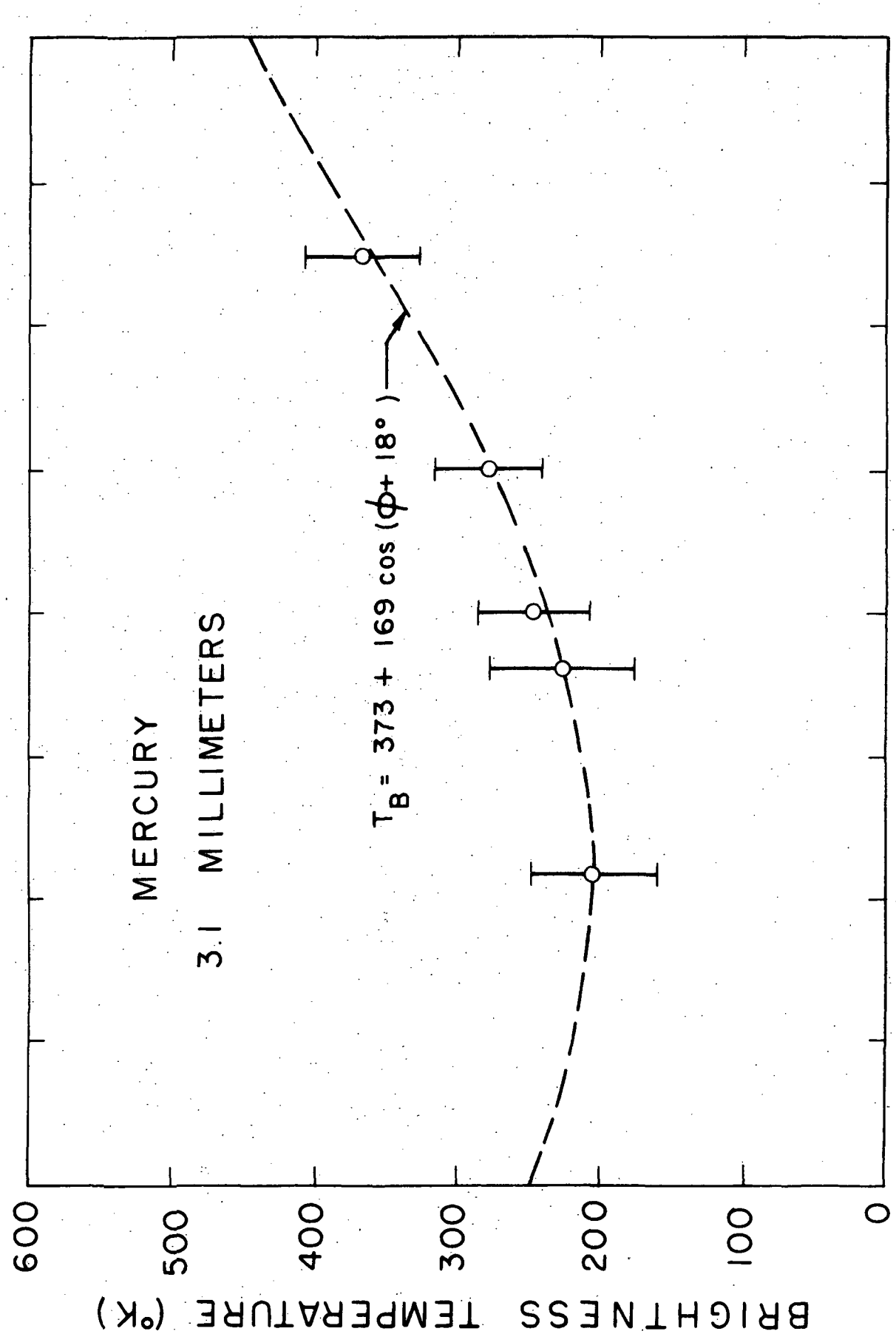
MERCURY
3.1 MILLIMETERS
$T_B = 373 + 169 \cos(\phi + 18°)$
BRIGHTNESS TEMPERATURE (°K)
600
500
400
300
200
100
0
120
140
160
180
200
220
240
260
280
PHASE ANGLE ϕ (°)

Fig. 8

high, thin clouds, but the results were erratic and are not tabulated below in Table V.

TABLE V

VENUS OBSERVATIONS

Wavelength (mm)	Date (1971)	T_B(°K)	σ_{T_B} (°K)	α(dB)	Method
3.1	3/21	356	43	.157	5
3.1	3/22	389	60	.188	5
3.1	3/23	411	58	.226	5
3.1	4/1	421	47	.324	5
3.1	4/5	456	59	.285	5
3.1	4/6	296	57	.269	5
8.6	6/15	503	102	.209	1

At 3.1 mm the weighted average is 386°K±26°K. Data were taken over too short a period of time to indicate the presence or absence of phase effects. The one observation at 8.6 mm is of poor accuracy but is included for the sake of completness. Taking into account the systematic errors, we obtain 386±33°K at 3.1 mm and 503±102°K at 8.6 mm for the disk brightness temperature of Venus.

3. Mars

Mars was observed on 5 days at 8.6 mm and on 6 days near opposition at 3.1 mm. The data are given below in Table VI.

TABLE VI

MARS OBSERVATIONS

Wavelength (mm)	Date (1971)	T_B (°K)	σ_{T_B} (°K)	α(dB)	Method
3.1	7/27	201	15	1.215	5
3.1	8/24	218	12	1.233	1
3.1	8/25	236	11	1.740	1
3.1	8/26	198	11	1.285	1
3.1	8/27	258	12	1.609	1
3.1	8/30	198	14	1.438	1
8.6	6/8	307	70	.118	1
8.6	6/9	142	44	.200	1
8.6	6/15	281	47	.209	1
8.6	6/16	172	42	.165	1
8.6	6/17	260	27	.228	1

The weighted average temperature at 3.1 mm is 217±11°K, and at 8.6 mm it is 224±38°K. Taking into account the gain and calibration uncertainties, the temperatures are 217±16°K at 3.1 mm and 224±38°K at 8.6 mm.

4. Jupiter

Measurements at 3.1 mm were conducted on nine days and at 8.6 mm on 4 days. The data from the individual days are given below in Table VII.

TABLE VII

JUPITER OBSERVATIONS

Wavelength (mm)	Date (1971)	T_B (°K)	σ_{T_B} (°K)	α(dB)	Method
3.1	3/21	198	6	.157	5
3.1	3/22	209	5	.188	5
3.1	3/23	210	6	.226	5
3.1	4/5	181	4	.285	5
3.1	4/6	186	4	.269	5
3.1	7/27	180	6	.844	5
3.1	8/24	157	6	.855	1
3.1	8/25	163	9	1.194	1
3.1	8/26	169	5	.711	1
8.6	6/4	138	6	.246	1
8.6	6/7	186	11	.118	1
8.6	6/8	186	10	.118	1
8.6	6/8	212	7	.118	1

The averages are 185±13°K at 3.1 mm and 174±20°K at 8.6 mm.

5. Saturn

The data on Saturn are given below in Table VIII.

TABLE VIII

SATURN OBSERVATIONS

Wavelength (mm)	Date (1971)	T_B (°K)	σ_{T_B} (°K)	α(dB)	Method
3.1	3/20	158	28	.219	1
3.1	3/21	149	19	.152	1
3.1	3/22	144	26	.187	1
3.1	3/23	147	19	.327	1
3.1	3/30	149	27	.385	1
3.1	4/5	157	26	.344	1
3.1	4/6	153	20	.197	1
3.1	4/23	144	19	.284	1
3.1	6/1	173	30	.261	5
8.6	6/10	101	42	.175	1
8.6	6/16	91	41	.182	1
8.6	6/17	113	40	.228	1

The average temperature at 3.1 mm is 151±11°K. At 8.6 mm the weighted average is 102±24°K. In the latter case the sample is too small to estimate the error from the data, so the statistical model combines the errors from the three days to estimate the overall error.

V. DISCUSSION OF RESULTS

A. General Considerations

Before we can discuss the implications of our measurements,

we must first discuss some general considerations which influence the interpretations of planetary spectra.

The first of these considerations is that the spectra of the planets may not be considered separately as if the various measurements were independent. The spectra of the planets are coupled through two effects. The first of these is due to the fact that the brighter planets, mainly Jupiter, are used as calibration sources for observations of the weaker ones. Jupiter is particularly favored for this purpose since its brightness is thought to be reasonably constant throughout the millimeter region. This assumption is not well founded in our view as the measurements are not thoroughly consistent, as will be discussed later, nor is there an established model of the Jovian atmosphere from which one might judge this assumption to be a priori valid. Even if one grants the assumption, the value one assumes for the Jovian temperature must be decided, presumably by referring to measured values. If one does a simple average of reported measurements of Jupiter in the region 1 mm $< \lambda <$ 1 cm, where the brightness temperature is presumed to be constant, one obtains the value 148±9°K (standard error) based upon 14 reported values including those in this report. If one considers only recent measurements, say later than 1967, the average is higher, 164±8°K, based upon 8 reported values. However the temperature usually assumed for Jupiter is in the range, 140-144°K. It is not our purpose to discuss the historical reasons for this here. Our point is that the use of Jupiter for a calibration source and the assumption of a low value for Jupiter's temperature have combined to influence the

spectra of all the planets. We will discuss these matters in detail in the following sections.

The second way the planetary spectra are coupled is through the systematic error of the observers. There are only a few radio telescopes which are used in the millimeter region for measurements of the planets, and, as discussed in the Appendix, the measurement errors of all sources for each facility would be correlated through the errors in antenna gain and thermal calibration scale. A clear example of this effect is revealed through a comparison of our planetary measurements at 3.1 mm and those made on the Aerospace Corporation 15' antenna at 3.3 mm. Table IX shows such a comparison and one sees that the Aerospace measurements are consistently lower than ours by about 19%.

TABLE IX

COMPARISON OF THE 3 MM PLANETARY BRIGHTNESS TEMPERATURES REPORTED HERE WITH THOSE OF EPSTEIN et al.

Planet	Mean Temperature (°K) This Paper	Epstein et al.	Ratio	Reference
Mercury	373±35	296±30	0.79±.11	Epstein et al. (1970a)
Venus	386±33	307±30	0.79±.11	Epstein et al. (1968)[a]
Mars	217±16	178±18	0.82±.10	Epstein et al. (1970b)
Jupiter	185±13	153±15	0.83±.10	Epstein et al. (1970b)
Saturn	151±11	125±13	0.83±.10	Epstein et al. (1970b)
Average			0.81±.02	

[a]This is the value reported at inferior conjunction.

Thus one has to bear in mind the possibility of correlated errors in considering all the planetary measurements made with a given radio telescope.

The second general consideration which we wish to discuss is that of phase effects, which have been reported in connection with Venus and Mercury. First, the measurement of a phase effect is extremely challenging from an observational point of view. One problem is maintaining a consistent calibration scale over an extended period of time. Second, and more important, is the problem of "synchronous noise." Just about every conceivable source of error (seasonal changes, solar heating of the antenna, solar interference, diurnal effects, elevation angle effects, signal-to-noise ratio) are correlated with the phase of the object being observed. Thus even when the observers are extremely careful there is a tendency to see systematic effects with changes in phase. This is what Sagan (1971) called "false positives" in connection with the phase effect of Venus. A second point we wish to discuss in connection with phase effects concerns the manner in which the data are taken and analyzed. The inner planets are closest to the earth at inferior conjunction, and it is hence at this time that the signal-to-noise ratio is best. There is a tendency to take too much of this "good data" and to give it too great a weight in the analysis of the data. Specifically the practice of weighting the data inversely to its relative variance allows the precise data near inferior conjunction to control the fit to the extent

of overriding the data near superior conjunction. Clearly the phase varying term should be determined by the difference between the values near the conjunctions (maximum and minimum temperatures), but the practices we have cited above allow the inferior conjunction data to overly influence this term as well, with the result that often the fit is poor near superior conjunction. This phenomenon also influences the average value for the planet. The way the data are taken and analyzed causes a strong correlation between the average value and the amplitude of the phase term. That is, consider a phase equation of the form

$$T(\varphi) = T_0 + T_1 \cos(\varphi + \delta) \qquad (4)$$

where

$T(\varphi)$ = The predicted phase curve (°K)

T_0 = The average planetary temperature (°K)

T_1 = The amplitude of the phase effect (°K)

φ = Synodic phase ($\varphi = 0°$ at superior conjunction)

δ = Phase shift, usually small, $< 20°$

The "good data" near inferior conjunction establishes $T(180°)$ very well, i.e.,

$$T_0 - T_1 \approx T(180°), \text{ well established.}$$

Then T_1 is established by variations in the data versus phase, again with the inferior conjunction data heavily weighted. Thus the average temperature is $\approx T(180°) + T_1$, and is highly correlated with the phase term. Another way to state this is that the average temperature of the planet one derives from the data in this way is model dependent. If one choses to disbelieve in the

phase effect, say in the case of Venus, then the best estimate of the planetary temperature is the value determined near inferior conjunction. The considerations discussed above will be factors in the discussion of planetary spectra which follows.

B. Planetary Spectra

1. Jupiter

We will discuss the spectrum of Jupiter first because of its importance as a calibration source. In Fig. 9 we show the spectrum of Jupiter at wavelengths shorter than 2 cm. The data are from Dickel et al. (1970), Newburn and Gulkis (1971), and some original sources, plus the data of this report.

At wavelengths longer than 2 cm, the nonthermal component is thought to be approximately 12°K and decreasing as $\lambda^{1.7}$; hence, the radiation is largely thermal in the region shown. Some of the values given near 2 cm have been corrected to remove the nonthermal component. The spectrum shows a dip at approximately $\lambda = 1.4$ cm with $T_B = 150 - 180$°K at short millimeter wavelengths. The general features of this spectrum agree with the models presented by Welch et al. (1966), Law and Staelin (1968), and Wrixon et al. (1971), which predict the dip in brightness temperature at 1.4 cm due to ammonia absorption in the higher, cooler region of the lower atmosphere.

The temperature of the Jovian atmosphere is not well established. Recent occulation results (Hubbard et al., 1971) lead to a minimum value of 130°K in the upper atmosphere. Sagan and Pollack (quoted in

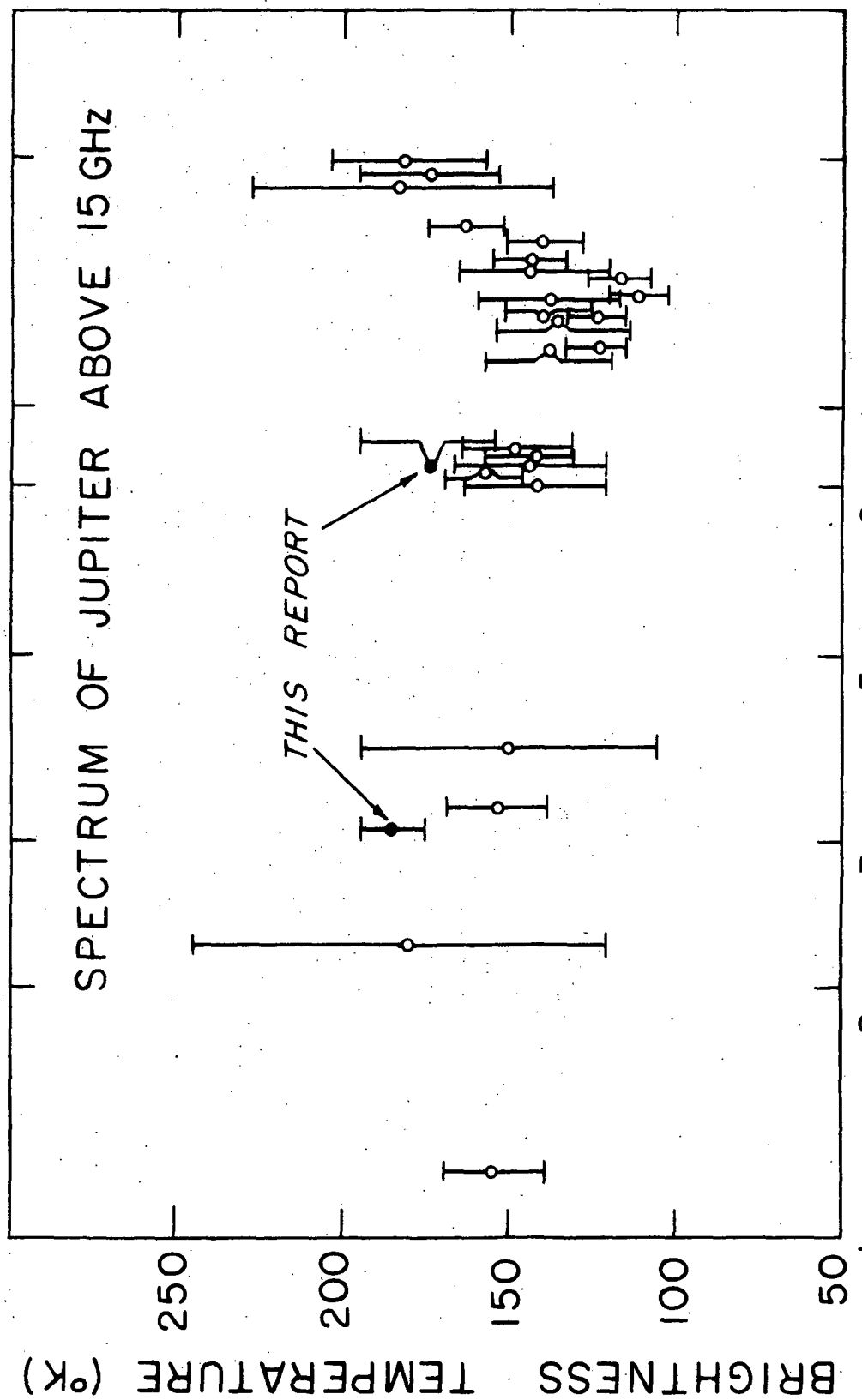
SPECTRUM OF JUPITER ABOVE 15 GHz
THIS REPORT
BRIGHTNESS TEMPERATURE (°K)
250
200
150
100
50
1mm
2mm
3mm
5mm
8mm
1cm
2cm
WAVELENGTH

Fig. 9

Kellerman and Pauliny-Toth, 1966) anticipate that the chief source of opacity and hence radiation in the planet's outer atmosphere would be saturated ammonia. The atmospheric level where the optical depth is on the order of unity corresponds to a temperature near the freezing point of ammonia, which is quoted to be 195°K. Our values are in agreement with this prediction. However, the data points added by this report are generally higher than previous measurements at nearby wavelengths, although our values are marginally compatible with them at the one to two sigma level. We are not embarrassed by this difference but feel that our measurements are valid.

Three methods are used in making planetary measurements at the wavelengths of concern. The Russian method (Kislyakov et al., 1962), used in a modified form by Law and Staelin (1968), depends on pattern measurements derived from solar limb crossings and thermal scaling based upon the moon. While this method yields results which strike us as reasonable, the precision is not very great.

A second method is to calibrate the antenna gain and receiver gain simultaneously through measurements of standard radio sources. Sometimes only one or two sources are used, sometimes more. Corrections are made for source size. Flux values for the standard sources must be extrapolated from the spectra measured at longer wavelengths. Some authors seem to prefer this type of calibration because relative values are more consistent than between "absolute" measurements. There are, however, several objectional features to this source of calibration in the short

cm and mm region. For one, extrapolating spectra into this region could yield trouble because of the possibility that the spectral index of the source might change in this region, as a number of sources do. Second, the standard sources become quite weak in the millimeter region and cannot currently be used at wavelengths less than 8 mm due to the smaller antennas and noisier receivers. Finally, spectra of the standard sources were determined by absolute measurements. It is hard to see why these older measurements are to be preferred over recent absolute measurements of the planets. Of course, in defining the spectra of the standard sources, one takes account of many measurements made with different antennas at different frequencies; nevertheless it is not uncommon to see the spectra revised significantly in the light of more recent measurements.

Finally, many measurements, such as those reported here, are absolute. The basic ingredients of such a measurement are the determination of the peak gain or efficiency of the antenna and the establishment of a thermal calibration scale, the latter component being the surer of the two. Some problems of gain calibration are described in Cogdell (1969a) and Davis (1970). Since the gain calibration measurements are difficult to make, radio telescopes are calibrated infrequently. Also, experimenters fall prey to the very natural temptation to overstate their accuracy. For these reasons, and no doubt others, absolute measurements have tended to disagree embarrassingly. Nevertheless, it is our view that absolute measurements can be made quite accurately, and we have sought to explain in our

various reports and publications the techniques and assumptions which underlie the present series of planetary measurements. Unfortunately, other authors have not reported similar details, so it is difficult to judge the foundations of their measurements.

The fact that the temperatures which we measure for the planets are higher than expected leads one to suspect that either our temperature scale is too high or else our assumed antenna efficiency is too low. The temperature scale is confirmed to better than 3% by the measurements on the Sun and Moon, as discussed earlier in this report. In the present section, we discuss the possibility that the antenna efficiency is underestimated in our evaluation. The efficiencies quoted, 53.7% at 3.1 mm and 67.2% at 8.6 mm, are based upon a measured efficiency at 2.2 mm, a calculated low frequency limit, and a theory of interpolation from Davis and Cogdell (1971). It is difficult to see how these values, particularly the 8.6 mm one, could be 20-25% low, as they are already rather high compared with the efficiencies claimed for other radio telescopes, particularly telescopes operating in the millimeter region. There is, in fact, a tendency to measure low. Most sources of error, e.g., pointing difficulties and telescope sag deterioration, tend to reduce the value one infers for the planetary temperature. In this connection, it is interesting to note that the values reported by a new facility are usually lower than their later, more carefully done measurements.

In the case of our own antenna, we have further reasons for assurance that the antenna efficiency is not understated, based upon

consideration of the main lobe efficiency. In any reflector antenna, the phase errors tend to fall into two classes: the small scale "random" errors caused by imperfections in the microstructure of the antenna surface and the large scale "systematic" errors caused by imperfections in the macrostructure of the antenna. The effect of the random errors, say, in transmitting with the antenna, is to scatter energy over a broad pattern depending on the characteristic scale of the errors. This effect is described by the Ruze (1966) tolerance theory. The effect of the systematic error is to scatter energy into and near the main lobe of the antenna, thus broadening the beam and smoothing out and raising the side lobe structure as described in Cogdell and Davis (1972). The relative effects of the two types of errors can be estimated by plotting the logarithm of the peak and main lobe efficiencies against the square of the frequency. As argued in Davis and Cogdell (1971) and Cogdell and Davis (1972), such a plot should yield straight lines. Figure 10 shows such a plot for our 16 foot antenna. In constructing the figure we have approximated the main lobe efficiency by using measured 3 dB beamwidths to estimate beam broadening. The interpretation of Fig. 10 is straightforward. The beam efficiency tolerance loss increases with frequency; this is due to the small scale phase errors only. The slope of this curve is indicative of the rms surface tolerance of the antenna and agreement is perfect between the slope calculated from the mechanically measured tolerance and the slope of the figure. The peak efficiency loss with frequency is due to all errors, random and systematic. The slope of this curve is indicative of the total

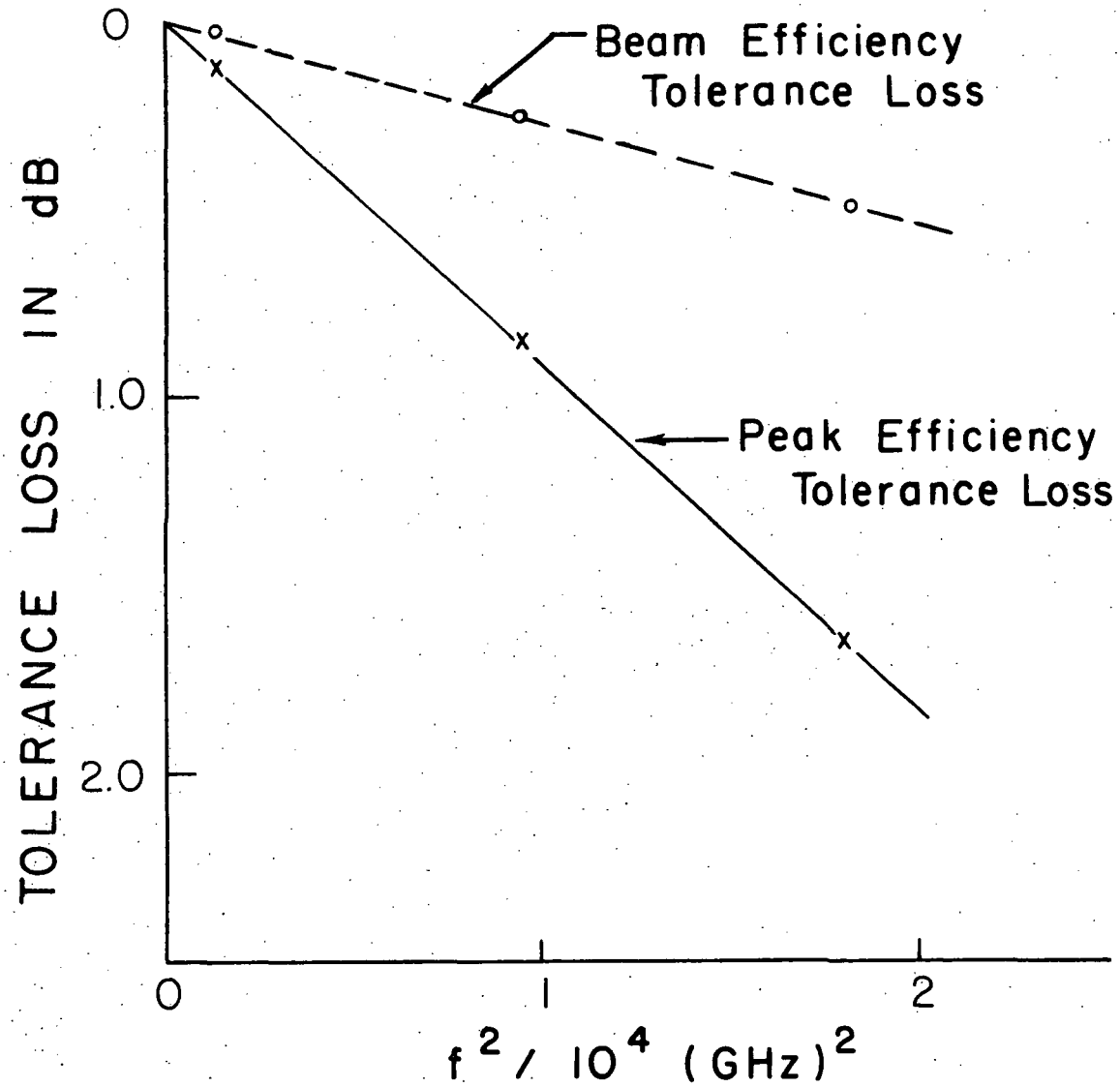

16 FOOT ANTENNA EFFICIENCY DIAGRAM

Fig. 10

tolerance of the antenna figure as defined by Spencer (1949) and indicates a tolerance twice that due to the random error alone. If the slope of the peak efficiency curve is raised (to give lower temperatures for the planets) the slope of the main beam efficiency curve must be increased by the same amount. But this is impossible because the slope of this curve already accounts for the measured mechanical tolerance of the antenna. To raise the slope would imply that the antenna figure is improving with time, which is unexpected to say the least. To raise the efficiency by 20% at 97 GHz would force the main beam efficiency to increase with frequency, which would, of course, be impossible. Thus our conclusion is that the peak efficiency values used in this report cannot be grossly underestimated. We accordingly assume that our planetary temperatures are correct and explore the implications of these higher values in interpreting planetary spectra in the millimeter region.

The structure and constituents of the Jovian atmosphere are not well determined. The most complete models of the atmosphere seem to be those of Trafton (1967). The Trafton model is described in Wrixon et al. (1971) and used in a calculation of the microwave emission in the frequency range between 20 GHz and 40 GHz, the vicinity of the ammonia complex. The calculated spectra agree in the main with the measurements reported in the same paper, although certain unknowns in the model, mainly associated with the effects of pressure on the ammonia absorption, are not distinguishable due to the uncertainty in the measured spectrum. The Trafton model is based upon an upper atmosphere in radiative equilibrium

at some effective temperature with a lower atmosphere in convective equilibrium. This results in a constant temperature region upwards from $\approx$ 25 km above the clouds with a temperature $\approx$ 90°K and an abiabatic lapse rate of $\approx$ 3.5°K/km on down to the clouds and below. The main opacity in the millimeter and long infrared region is due to ammonia and hydrogen molecules. At frequencies below 1 mm only the ammonia is important, according to Wrixon et al. (1971).

The spectrum calculated by Wrixon et al. (1971) shows the expected temperature at 35 GHz to be about 150°K and gradually increasing with frequency. Their own measurement at 35.5 GHz is 157±8(2σ)°K. Unfortunately the calculated spectrum is not extended beyond 40 GHz, although it is probable that the calculated curve would not rise to 185°K at 100 GHz, as our measurement of 185±13(1σ)°K requires. The agreement of the measurements by Wrixon et al. (1971) with their calculated spectrum is better below 30 GHz than above, where they measure a steeply increasing temperature (One must bear in mind that their error bars are at the 2σ or 95% confidence level.). It is not surprising the agreement is not perfect in view of the many assumptions underlying the calculations. In particular the temperature of the atmosphere in radiative equilibrium is assumed to be 120°K instead of the 134°K measured by Aumann et al. (1969). The higher effective temperature would have two effects on the calculations: temperatures would generally be higher in the atmosphere, thus raising the calculated emission temperature at millimeter wavelengths, and the ammonia opacity would decrease, the absorption varying as $T^{-9/2}$ in

the upper tail of the absorption line. This would cause the atmopshere to be more transparent and hotter emission temperatures would be expected.

We suggest that the model calculations (Trafton, 1972) be repeated for T_e = 134°K. Also the ammonia absorption in simulated Jovian atmospheres should be measured, much in the manner that Ho et al. (1966) simulated Venusian atmospheres. Finally we plan to measure Jupiter's brightness temperature at 2 mm wavelength, since this would support or contradict the upward trend which we measure at 3 mm wavelength.

2. Mercury

Passive microwave observations are capable of providing information as to the thermal and electrical properties of the Mercurian epilith. The absolute value of the mean temperature, the amplitude of the phase varying term, and the phase lag of insolation behind temperature are determined by the thermophysical nature of the surface material. A knowledge of these quantities, particularly at several different wavelengths, allows one to test the validity of existing theoretical models.

The best fit curve to our 3.1 mm observations, illustrated in Fig. 8, is given by

$$T_B = 373 + 169 \cos (\Phi + 18°)\ °K \qquad (5)$$

Since the data cover only a limited range of phase angle, it is difficult to meaningfully estimate the true errors. Note, however, that data were

taken at the phase angles where the minimum and mean temperatures are expected to occur. Thus the errors are approximately the error of one observation, or about 35°K. Epstein et al. (1970a) reported the best three parameter fit to their extensive observations at 3.3 mm as

$$T_B = \underset{\pm 7}{296} + \underset{\pm 9}{130} \cos (\Phi + \underset{\pm 5}{18°}) \text{ °K} \qquad (6)$$

The percent phase variation and phase lag reported here are in excellent agreement with this earlier result. However, their absolute temperatures are about 19% lower than the values reported here. The value of δ/λ implied by our results may be determined by the procedure summarized by Klein (1968). Here δ/λ is the ratio of electrical to thermal skin depths normalized by the wavelength of observation. As in Epstein's case, our value for the ratio of the mean temperature to the amplitude of the phase term is consistent with a δ/λ of about 1.3 cm^{-1}.

A larger magnitude of the absolute mean temperature near 3 mm leads to a revision of the microwave spectrum given in Morrison and Klein (1970). Table X, adapted from Morrison and Klein (1970), lists the mean observed temperatures at longer wavelengths. The data of Golovkov and Losovskii (1968) is so much higher than all other measurements that we choose to exclude it. Similarly, the result of Kaftan-Kassim and Kellermann (1967) at 1.95 cm will not be considered here since it is inconsistent with the more recent observations of Morrison and Klein (1970) at the same wavelength on the same instrument. Figure 11 is a plot of the observed absolute mean disk brightness temperature as a function of

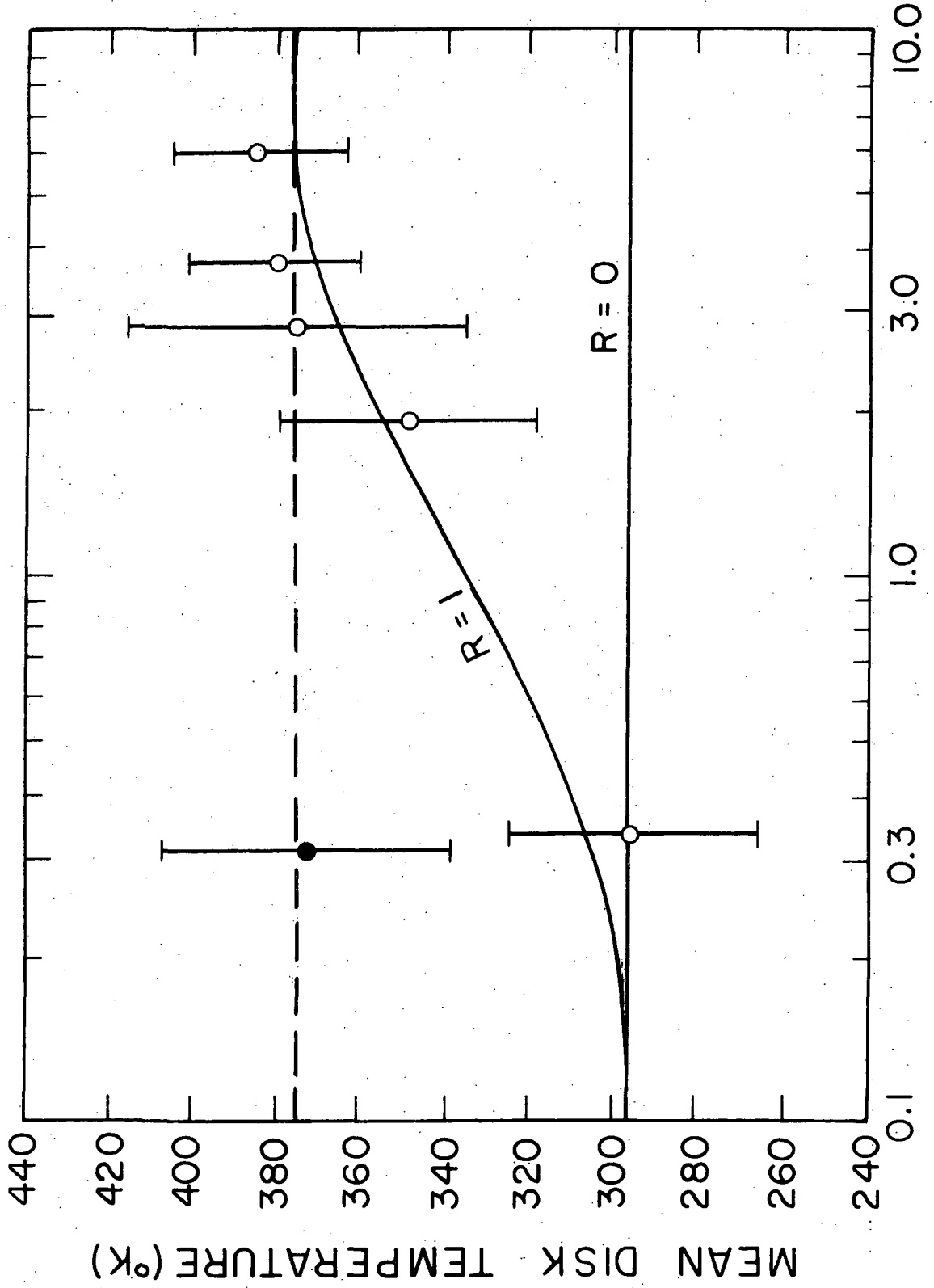

MEAN DISK TEMPERATURE OF MERCURY

Fig. 11

TABLE X

REPORTED MEAN TEMPERATURES OF MERCURY

Wavelength (cm)	Mean Temperature[a] (°K)	Reference
0.31	373±35	This paper
0.33	296±30	Epstein et al. (1970a)
0.80	530±159	Golovkov and Losovskii (1968)
1.95	288±30	Kaftan-Kassim and Kellermann (1967)
1.95	350±30	Morrison and Klein (1970)
2.82	375±40	Medd (1968)[b]
3.75	380±20	Klein (1970)
6.00	385±20	Morrison and Klein (1970)

[a]The uncertainty is the 1-σ total system uncertainty including all calibration errors.

[b]This measurement was quoted by Morrison and Klein (1970).

wavelength. The solid curves are spectra predicted by the model of Morrison (1969a). The curve for R = 0 is the predicted spectrum assuming a temperature independent thermal conductivity. The curve for R = 1 is produced by a conductivity in which the radiative term is equal to the contact conductive term. Our measurement indicates a mean brightness temperature of 373±35°K at 3.1 mm. This seems inconsistent with the earlier result at 3.3 mm of 293±30°K by Epstein et al. (1970a). The conclusion by Morrison and Klein (1970) that the mean temperature increases with depth, and thus

that radiative conduction is important, hinges critically on the 3 mm observations of Epstein et al. (1970a). Note, however, if our result is substituted, the spectrum appears flat from 3 mm to 6 cm. The dashed line in Fig. 11 represents a constant mean temperature of 375°K. It is clearly consistent with all the included data except that of Epstein et al. (1970a).

The flat planetary spectrum is consistent with a thermal conductivity in which the contact term dominates the radiative term. Thus the thermal conductivity appears to be independent of temperature. Indeed, Epstein et al. (1970a) have noted that their extensive observations were best fit by Morrison's (1969a) model with a temperature independent conductivity. The constant mean temperature of 375°K, however, is higher than that predicted by Morrison's model for a temperature independent thermal conductivity. Values of the albedo, microwave emissivity, or midnight equatorial temperature different from those assumed by Morrison (1969a) could produce a uniformly greater mean temperature. In particular, the midnight infrared surface temperature is poorly known. Murray (1967) has observed an upper limit of 150°K while Soter (1966) reported a lower limit of 180°K. A value greater than that assumed by Morrison (1969a) would increase the mean brightness temperature. In view of the large uncertainties of the assumed quantities, it seems possible to fit the revised spectrum with Morrison's model using plausible material properties.

Taking into account our recent determination of the absolute mean temperature of Mercury, the spectrum appears flat with a constant

mean brightness temperature near 375°K between 3 mm and 6 cm. Thus the thermal conductivity of the epilith is essentially temperature independent. The ratio of electrical to thermal skin depths is near 1.3 at 1 cm wavelength.

3. Venus

The microwave emission spectrum of Venus depends upon the thermal and electrical properties of its surface and atmosphere. The passive radio measurements, combined with radar and interferometric data, indicate the following picture. At long wavelengths, say $\lambda \gg 3$ cm, the atmosphere is optically thin and one sees the hot ($\approx$ 700°K) surface of the planet. At $\lambda = 3.8$ cm, the atmosphere's optical thickness is approximately unity (Muhleman, 1969). In the region 2 cm $< \lambda <$ 3 cm the atmosphere becomes optically thick and the emission spectrum drops to a cooler temperature (300-400°K). There seems to be a particularly sharp drop in the temperature between 3 cm and 1.5 cm, which is interpreted by Pollack and Morrison (1970) to indicate the presence of H_2O in the atmosphere.

The microwave spectrum of Venus is pictured in Fig. 12. The basic data are adapted from Pollack and Morrison (1970) with several changes. The phase effects have been discounted and hence the values near inferior conjunction were used. The absence of a strong phase effect seems now well established, as discussed by Sagan (1971). This change affected the points of Epstein et al. (1968) at 3.4 mm and Kalaghan et al. (1968) at 8.6 mm. We also corrected the measurements of Efanov et al. (1969) at 2.25 mm and 8 mm in accordance with the Jovian measurements

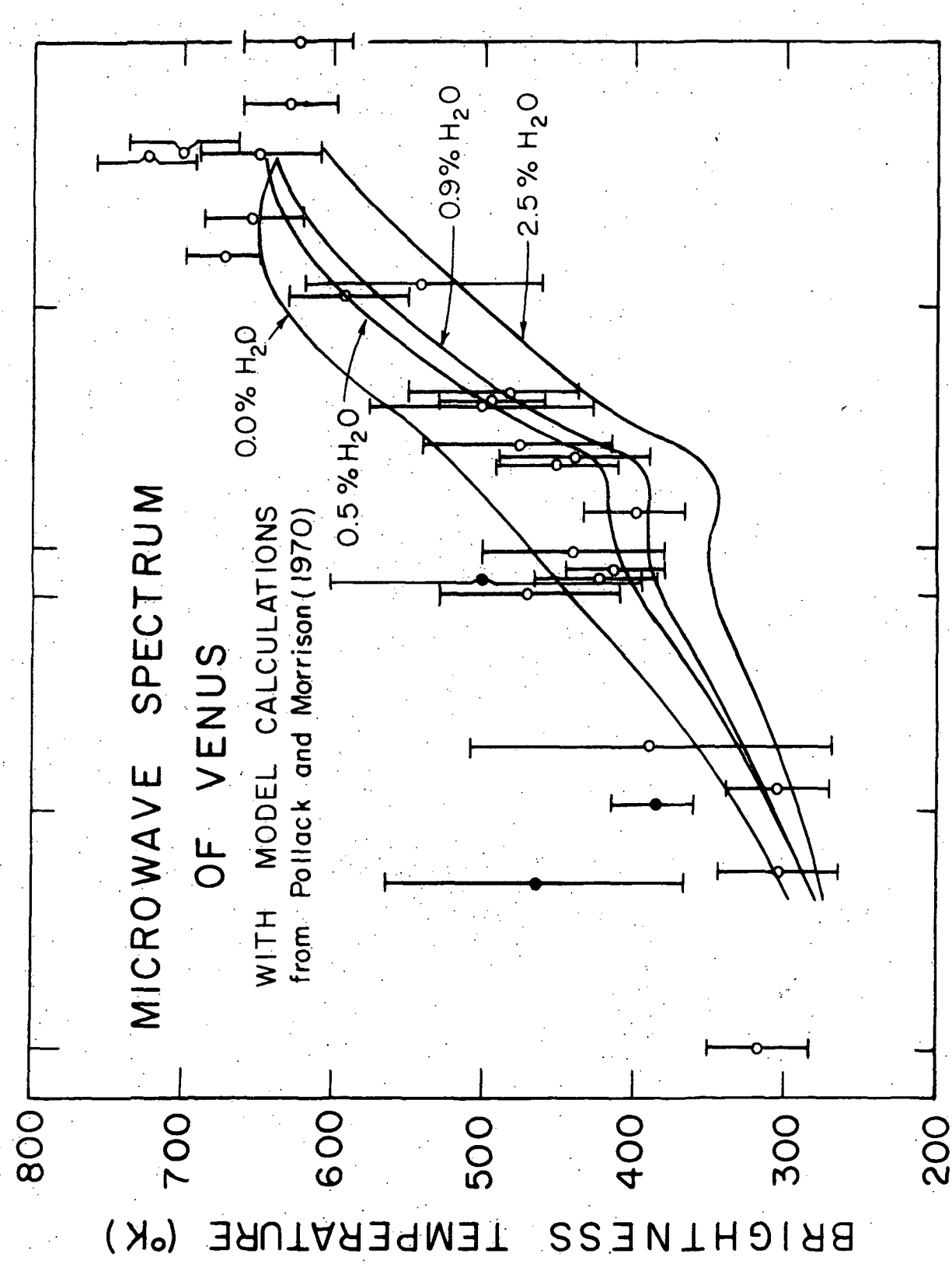
MICROWAVE SPECTRUM
OF VENUS
WITH MODEL CALCULATIONS
from Pollack and Morrison (1970)
0.0% H_2O
0.5% H_2O
0.9% H_2O
2.5% H_2O
BRIGHTNESS TEMPERATURE (°K)
800
700
600
500
400
300
200
1 mm
3 mm
8mm
1cm
3 cm
10cm
WAVELENGTH

Fig. 12

in this paper, as their Venus measurements were made relative to Jupiter. In correcting the 2.25 mm measurement of Efanov et al. (1969) we used 185°K for Jupiter instead of 150°K which they use. Interestingly, this correction brings their measurement relative to Jupiter into agreement with their measurement relative to the Sun.

The solid lines on Fig. 12 are model spectra from Pollack and Morrison (1970) computed for 90% CO_2, the remainder N_2 and H_2O as indicated on the figure. Temperature and pressure profiles used in the calculation are derived from the Venera probes and Mariner 5 data. The basic concern of Pollack and Morrison was to fit the spectrum in the 1-3 cm region and to account if possible for the reported falling off of the spectrum at longer wavelengths. Little attention was paid to the spectrum at wavelengths less than 1 cm.

It is, of course, the millimeter region which concerns us in this report. In Fig. 12 it is clearly seen that all the points near 8.6 mm fall above the spectrum which Pollack and Morrison (1970) predict (0.5% H_2), although the disagreement is not serious. The point added by this report is higher than the nearby points and indicates the trend more strongly.

Our point at 3.1 mm is substantially above the predicted spectrum. The point of Epstein et al. (1968) agrees with the predicted spectrum, but we feel that this point is about 19% low, as indicated by Table IX. The 2.25 mm point of Efanov et al. (1969) is higher than the predicted spectrum, although compatible with it, after correction for a higher reference temperature of Jupiter. In view of the possible increase

in Jupiter's temperature between 8.6 mm and 3.1 mm (174°K to 185°K) it might be reasonable to assign a higher temperature to Jupiter at 2.25 mm, which would raise the Venus measurement even higher. Furthermore we have made a tentative measurement of Venus at λ = 2.14 mm and obtain 465±100°K. Thus our conclusion is that the measured values at 2-3 mm are higher than the values predicted by Pollack and Morrison's best model by 20%.

The calculations of the emission spectrum of Venus in Pollack and Morrison (1970), as well as other papers on this subject utilizing a model for microwave absorption in Venusian-type atmospheres, are based upon the laboratory measurements of Ho et al. (1966). These measurements were made at wavelength of 3.24 cm and extrapolated to other wavelengths by assuming that losses vary as the square of the frequency. To support this scaling, they argue that the frequencies of interest are well below resonance effects and cite measurements to support this scaling law. However, the cited measurements of Frenkel and Woods (1966) of CO_2 at 1 mm and 2 mm (upper limit only) fall $\approx$ 50% below the values extrapolated from Ho et al. (1966). The above comments apply strictly to a 100% CO_2 atmosphere but presumably apply to mixed atmospheres as well. Hence, one would expect that emission temperatures calculated from Ho et al. (1966) model would give values which are too low in the region λ < 1 cm, which we see to be the case. We have made a rough calculation of the effect to be expected in the Pollack and Morrison (1970) model if the opacity is reduced 50% at 3.1 mm and find an increase of about 30°K. Thus this effect only marginally

accounts for the higher measured values in the 2-3 mm range. This would argue weakly for the absence of much H_2O and O_2 in the region where the 2-3 mm radiation originates.

4. Mars

As pointed out by Morrison et al. (1969) and by Troitskii (1970), the microwave spectrum of Mars may be used to determine some of the thermal and electrical properties of its surface material. However, considerable confusion has arisen as to the interpretation of published brightness temperatures, particularly in the millimeter region. The solution of the one-dimensional equation of heat conduction predicts that observed brightness temperatures should increase as the wavelength decreases. Epstein (1971) has summarized the available data and concludes that the spectrum appears flat or slightly convex. We measured the disk brightness temperatures of Mars at 3.1 mm and 8.6 mm wavelengths and obtained 217±16°K and 224±38°K, respectively. As a result of these and other data, we conclude that the spectrum of Mars is of the form suggested by simple thermal models and that the confusion in interpreting the spectrum resulted from poor quality data and incorrect assumptions as to the millimeter brightness temperature of Jupiter.

Table XI, adapted from Epstein (1971), lists the radio observations of Mars. We have included the recent results of Efanov et al. (1971) at 2.3 mm and 8.15 mm, Kalaghan and Telford (1971) at 8.57 mm, and the observations reported in this paper. In addition we have revised measure-

TABLE XI[a]

RADIO OBSERVATIONS OF MARS

λ (cm)	T_B C[b] (°K)	Uncertainty[c] (°K)	Calibration Standard(s)	Reference
0.12	171	±31	T_B(Moon) = 213±24°K	Low and Davidson (1965)
0.14	234	±66	T_B(Jupiter) = 185±20°K	Kostenko et al. (1970)
0.23	314	±35	T_B(Jupiter) = 185±20°K	Efanov et al. (1971)
0.31	217	±16	Antenna parameters + receiver calibration	This paper
0.33	178	±18	T_B(Sun) = 6600±200°K + antenna parameters	Epstein et al. (1970b)
0.815	252	±34	T_B(Jupiter) = 174±20°K	Efanov et al. (1971)
0.822	209	±25	T_B(Jupiter) = 174±20°K	Kuzmin et al. (1971)
0.857	214	±25	T_B(Jupiter) = 174±20°K	Kalaghan and Telford (1971)
0.86	224	±38	Antenna parameters + receiver calibration	This paper
0.95	215	±26	T_B(Jupiter) = 174±20°K	Pauliny-Toth and Kellermann (1970)
0.95	211	±14	S(Vir A) = 18.5 f.u. S(3C 123) = 3.0 f.u. S(DR 21) = 10.0 f.u. S(NGC7027) = 6.1 f.u. S(W49) = 54.0 f.u. S(W51) = 74.0 f.u.	Hobbs and Knapp (1971)
1.55	165	±33	T_B(Jupiter) = 140±14°K	Hobbs et al. (1968)
1.65	197	±16	S(Vir A) = 26 f.u.	Mayer and McCullough (1971)
1.85	187	115	S(Vir A) = 28 f.u.	Klein (1971)

λ (cm)	$T_B C$[b] (°K)	Uncertainty[c] (°K)	Calibration Standard(s)	Reference
1.95	186	±20	T_B(Jupiter) = 182±17°K	Pauliny-Toth and Kellermann (1970)
2.7	186	±12	S(Vir A) = 38.5 f.u.	Mayer and McCullough (1971)
3.14	211	±28	Antenna parameters +	Giordmaine et al. (1959)
3.75	206	±12	S(Vir A) = 50 f.u.	Dent et al. (1965)
3.75	210	±11	S(Vir A) = 50 f.u.	Klein (1971)
6.0	196	±27	S(Hydra A) = 13.0 f.u.	Kellermann (1965)
6.0	188	±60	S(3C123) = 16.32 f.u. S(Vir A) = 72.1 f.u. S(3C348) = 11.89 f.u.	Hughes (1966)
10.0	184	±18	S(3C123) = 24.7 f.u.	Drake (1962)
11.1	201	±18	S(Hydra A) = 24.3 f.u.	Stankevich (1970)
11.3	170	±19	S(Hydra A) = 24.7 f.u.	Kellermann (1965)
12.5	240	±42	S(3C33) = 8.6 f.u. S(3C245) = 2.22 f.u. S(3C267) = 1.42 f.u. S(3C295) = 13.3 f.u.	Muhleman and Sato (1965)
21.2	233	±65	S(Hydra A) = 36.3 f.u.	Davies and Williams (1966)
21.3	163	±35	S(Hydra A) = 36.3 f.u.	Kellermann (1965)

[a] Adapted from Epstein (1971).

[b] C is the factor used to correct the brightness temperature to a heliocentric distance of 1.524 a.u. ($=r_o$). For observations at $\lambda < 1$ cm, $C = (r/r_o)^{1/2}$; for 1 cm $\leq \lambda <$ 10 cm, $C = (r/r_o)^{1/4}$; and for $\lambda \geq 10$ cm, $C = 1$.

[c] This uncertainty is the 1-σ total system uncertainty including all calibration errors. All uncertainties in this paper are one standard deviation.

ments made relative to Jupiter. The quoted 1-σ errors include uncertainties in antenna gain and calibration source strength.

As discussed previously, the spectra of the planets are not independent. For instance, more than half the millimeter Mars observations listed in Table XI were made relative to Jupiter. Incorrect assumptions as to the brightness temperature of Jupiter will lead to errors in the calculated absolute Mars temperatures. Accordingly, we have revised the millimeter relative measurements using the more accurate Jupiter temperatures reported in this paper. We measured the disk brightness temperatures of Jupiter to be 185±13°K at 3.1 mm and 174±20°K at 8.6 mm. All the 8 mm and 9 mm relative measurements listed in Table XI have been revised assuming 174±20°K for Jupiter. The 1.4 mm and 2.3 mm relative measurements were revised assuming Jupiter to be 185±20°K. Note that a more conservative statistical error has been adopted since we measured Jupiter at a different wavelength. The 1.95 cm observation by Pauliny-Toth and Kellermann (1970) has been revised assuming the total thermal and non-thermal brightness temperature of Jupiter to be 182±17°K (Dickel et al., 1970). Figure 13 is a plot of the revised radio spectrum of Mars using the data from Table XI.

We now turn to the problem of interpreting the spectrum in terms of the homogeneous thermal model. This model predicts that the observed brightness temperature should increase as the wavelength decreases, since the radio emission at shorter wavelengths originates nearer the surface. We assume that the disk-averaged surface temperature

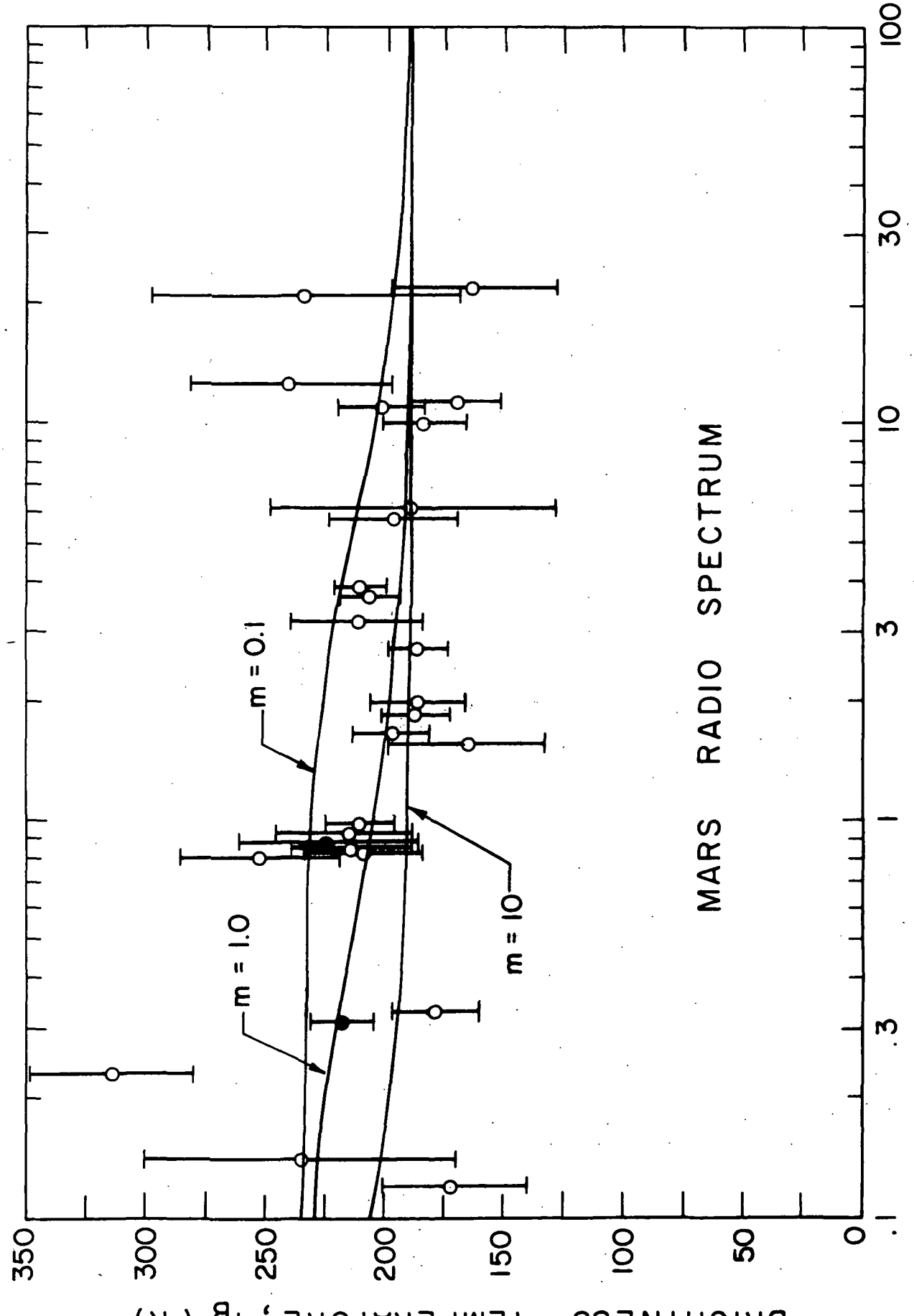
MARS RADIO SPECTRUM
BRIGHTNESS TEMPERATURE, T_B (°K)
WAVELENGTH, λ (cm)
m = 0.1
m = 1.0
m = 10
350
300
250
200
150
100
50
0
.1
.3
1
3
10
30
100

Fig.13

is given by the infrared value T_{IR} = 235°K (Petit and Nicholson, 1924, Menzel et al., 1926, Sinton, 1964, and Moroz, et al., 1969). The effective temperature between 1.5μ and 350μ was measured to be 234±7°K by Aumann et al. (1969). The temperature observed at long wavelengths should be a constant value unaffected by diurnal variations in insolation. As suggested by Epstein (1971), we adopt the value T_{∞} = 189°K, which is the weighted average of the values in Table XI for $\lambda \geq 6$ cm. According to Troitskii (1970) the Martian brightness temperature at opposition at a wavelength λ is given by

$$T_B(\lambda) = T_{\infty} + (T_{IR} - T_{\infty}) \cos \xi \frac{1 + \delta - \delta \tan \xi}{1 + 2\delta + 2\delta^2} \qquad (7)$$

where $\xi = 10°$, the maximum phase shift of the radio emission with respect to the maximum insolation. Here δ, the ratio of electrical to thermal skin depths, is assumed to be equal to $m\lambda$, where m is a constant (Troitskii, 1967).

We used the revised radio spectrum of Mars to infer probable values of $m = \delta/\lambda$. From this range in m we calculated values for the physical parameters of the surface material. Superimposed on the spectrum of Fig. 13 are the theoretical curves predicted by the homogeneous thermal model for several values of m. Values of the parameter which result in a reasonably good fit to the data are $m = 1.0^{+1.0}_{-0.5}$ cm^{-1}. However, several of the millimeter temperatures are inconsistent with the theoretical spectra. The data of Efanov et al. (1971) at 2.3 mm are higher

than other measurements at similar wavelengths. The data of Low and Davidson (1965) at 1.2 mm and of Epstein et al. (1970b) at 3.3 mm are below the temperature reported here at 3.1 mm. As suggested earlier in this paper, the discrepancy between our 3 mm observations and those of Epstein appears due to a difference in calibration, since the planetary temperatures differ by a constant amount ($\approx$ 19%). Epstein (1971) assumes as a primary calibration standard the temperature of the Sun to be 6600±200°K at 3.3 mm. In this paper we report our measured value of 6573±218°K at 3.1 mm. The excellent agreement of these two values rules out any significant differences in the thermal scale used to calibrate the receiver output in terms of antenna temperature. Low and Davidson (1965) assume the mean brightness temperature of the center of the Moon to be 213±24°K as their calibration standard at 1.2 mm. We have observed a point near the Moon's mean center during a lunation and integrated the resulting curve in Fig. 7 to obtain the mean temperature at 3.1 mm. Our value of 215±6°K is in excellent agreement with that assumed by Low and Davidson (1965) since this quantity is expected to be essentially independent of wavelength. Here also the thermal scales appear to be consistent. The discrepancy, then, must be ascribed to errors in determining the peak antenna gain. Note that observing an extended source such as the Sun or Moon provides no direct information as to the peak antenna gain. Our method of measuring the antenna gain relative to a standard gain horn (Davis and Cogdell, 1971) results in more precise absolute measurements.

If the net temperature gradient in the subsurface Martian material is negligible, if the microwave emissivity is independent of wavelength, and if the influences of the Martian atmosphere are negligible, then $\delta = m\lambda$ can be determined from the shape of the radio spectrum. The revised spectrum of Fig. 13 is best fit by the theoretical curve for

$$m = 1.0 \begin{matrix} +1.0 \\ -0.5 \end{matrix} \text{ cm}^{-1} \tag{8}$$

The quantity δ is the ratio of electrical to thermal skin depths. As is known, the electrical skin depth is given by

$$\ell_e = \frac{\lambda}{2\pi\, \epsilon^{1/2} \tan \Delta} \tag{9}$$

where λ is the wavelength, ϵ is the dielectric constant, and $\tan \Delta$ is the loss tangent of the surface material; the thermal skin depth is

$$\ell_t = \left[\frac{kP}{\pi \rho c}\right]^{1/2} \tag{10}$$

where k is the thermal conductivity, ρ is the density, and c is the specific heat capacity of the Martian soil, and P is the diurnal period. Thus $m = \delta/\lambda$ is also given by

$$m = \frac{c\gamma}{2b\,(\epsilon \pi P)^{1/2}} \tag{11}$$

where $\gamma = (k\rho c)^{-1/2}$ is the inverse thermal inertia and $b = \tan \Delta/\rho$ is the specific loss tangent. According to Neugebauer et al. (1971) for Mars a mean value of $\gamma \approx 170$ cal^{-1} cm^2 sec$^{1/2}$ °K is consistent with infrared

Mariner observations. The density $\rho \approx 1.2$ gm cm^{-3} has been suggested for the topsoil of Mars by Pollack and Sagan (1970). For most rocks $c \approx 0.17$ cal gm^{-1} $°K^{-1}$, and thus the thermal conductivity $k \approx 1.7 \times 10^{-4}$ cal cm^{-1} sec^{-1} $°K^{-1}$. Laboratory measurements by Fountain and West (1970) have shown that $k \approx$ constant independent of temperature for the Martian epilith. The first harmonic of the thermal wave penetrates to depths $\ell_t \approx 5$ cm for the diurnal variation and $\ell_t \approx 120$ cm for the seasonal variation. The electromagnetic wave penetrates to a depth $\ell_e = \ell_t m\lambda \approx 5\lambda$. The dielectric constant $\epsilon = 2.6 \pm 0.8$ has been given by Evans and Hagfors (1968) from radar reflectivity measurements. Our determination of m from the shape of the radio spectrum leads to values for the specific loss tangent of

$$b = (1.7^{+2.4}_{-1.0}) \times 10^{-2} \text{ cm}^3 \text{ gm}^{-1} \qquad (12)$$

Thus the Martian surface appears to be a good dielectric. Since the lunar value is $b = 0.008$ (Troitskii, 1967), the Martian epilith appears to have electrical properties similar to those of the lunar soil.

We conclude that the microwave spectrum of Mars was confused because of inaccurate absolute measurements of Mars and Jupiter at millimeter wavelengths. The spectrum does turn up at shorter wavelengths and, within the accuracy of the measurements, is fit by the homogeneous thermal model with material properties similar to those of the Moon. The presence of a thin layer of liquid water suggested by Sagan and Veverka (1971) is thus highly unlikely, although, as demonstrated

by Ingersoll (1971), concentrated solutions of strongly deliquescent salts could possibly occur.

5. Saturn

The disk temperature of Saturn has been measured at wavelengths between 1.5μ and 73.5 cm. The published observations are tabulated in Table XII and plotted in Fig. 14. Our values of 151±11°K at 3.1 mm and 102±24°K at 8.6 mm are seen to be in reasonable agreement with other results at similar wavelengths.

The observed microwave spectrum of Saturn is consistent with thermal emission from a deep atmosphere with a large temperature gradient and an opacity which depends on wavelength. No significant radiation has been observed except from the visible disk (Berge and Read, 1968), and the radiation appears to be purely thermal in origin (Davies et al., 1964, and Kellermann, 1966). At microwave frequencies the rings should not radiate significantly (Wrixon and Welch, 1970) and their effect has been neglected.

Probable main constituents of the atmosphere of Saturn are H_2, CH_4, NH_3, and possibly He. Gulkis et al. (1969) conclude that a cosmic abundance of ammonia is consistent with the longer wavelength radio observations. McAdam (1969) has reported a disk temperature of 1690±430°K at 73.5 cm. If one assumes an adiabatic lapse rate of 1.62°K/km in the lower atmosphere (Gulkis et al., 1969), this temperature implies an ammonia mixing ratio of about $(3\pm1) \times 10^{-4}$, in excellent agreement with the radio observations at 21 cm and the cosmic abundance ratio of 3.7×10^{-4}

TABLE XII

RADIO OBSERVATIONS OF SATURN

λ(cm)	T_B(°K)	Uncertainty[a](°K)	Reference
.12	140	± 15	Low and Davidson (1965)
.31	151	± 11	This paper
.32	97	+ 52 - 42	Tolbert (1966)
.33	125	± 13	Epstein (1970b)
.43	103	+ 70 - 64	Tolbert (1966)
.80	132	± 9	Salomonovich (1965)
.85	151	± 7	Wrixon and Welch (1970)
.86	96	± 20	Braun and Yen (1968)
.86	116	± 30	Tolbert (1966)
.86	102	± 24	This paper
.955	126	± 6	Hobbs and Knapp (1971)
.98	138	± 6	Wrixon and Welch (1970)
1.18	131	± 5	Wrixon and Welch (1970)
1.27	127	± 6	Wrixon and Welch (1970)
1.46	133	± 8	Wrixon and Welch (1970)
1.53	141	± 15	Welch et al. (1966)
1.9	140	± 15	Kellerman (1970)
3.12	137	± 12	Berge (1968)
3.45	144	± 30	Cook et al. (1960)[b]
3.75	168	± 11	Seling (1970)
6.0	190	± 45	Hughes (1966)
6.0	179	± 19	Kellermann (1966)
9.0	165	± 25	Berge and Read (1968)
9.4	177	± 30	Rose et al. (1963)
10.0	196	± 55	Drake (1962)
10.7	172	± 20	Berge and Read (1968)
11.3	182	± 18	Davies et al. (1964)
11.3	196	± 20	Kellermann (1966)
21.2	286	± 37	Davies and Williams (1966)
21.3	303	± 50	Kellermann (1966)
49.5	385	± 65	Yerbury et al. (1971)
70.0	<1250		Gulkis et al. (1969)
73.5	1690	±430	McAdam (1969)

[a]This uncertainty is the 1-σ total system uncertainty including all calibration errors. All uncertainties in this paper are one standard deviation.

[b]This measurement has been revised by Seling (1970).

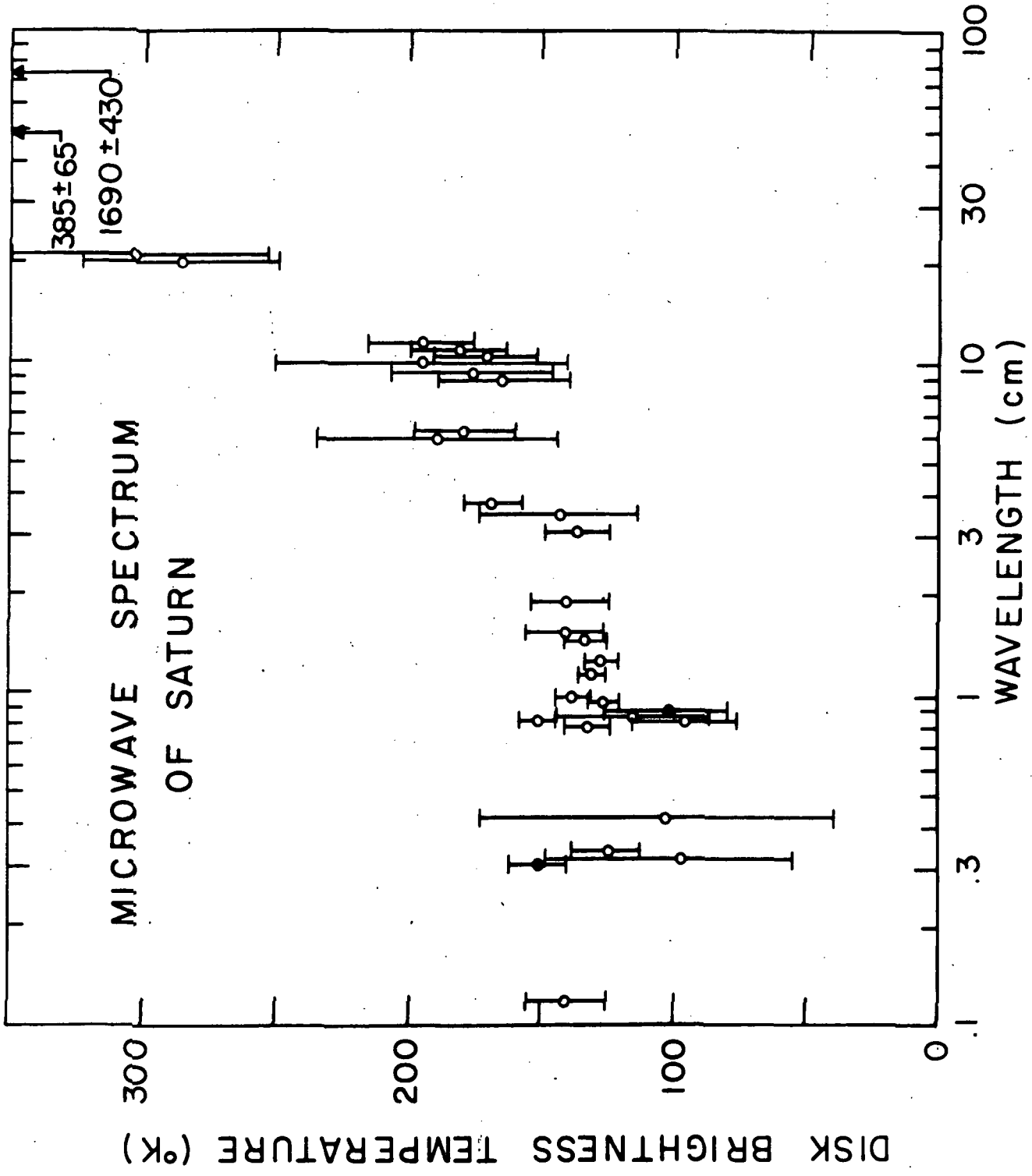
MICROWAVE SPECTRUM
OF SATURN
385±65
1690±430
DISK BRIGHTNESS TEMPERATURE (°K)
300
200
100
0
.1
.3
1
3
10
30
100
WAVELENGTH (cm)

Fig. 14

for a hydrogen-rich atmosphere (Field, 1959). Wrixon and Welch (1970) have concluded that ammonia should provide the chief source for atmospheric opacity at moderate pressure near 1 cm wavelength. The exact form of the microwave spectrum is determined by the dependence of ammonia absorption on the variations of temperature and pressure with depth in the atmosphere and on the presence of other atmospheric constituents. Wrixon and Welch (1970) have detected a distinct minimum in the spectrum near the 1.3 cm inversion band of ammonia. Their results are consistent with a cosmic abundance of ammonia and an effective temperature of 100°K.

The effective disk temperature of a rapidly rotating planet with a Bond albedo A at a distance a from the Sun in astronomical units is given approximately by

$$T_{eff} = 394\,(1 - A)^{1/4}\,(2a)^{1/2}\ ^{\circ}K \qquad (13)$$

If we assume A = 0.45 for Saturn, by analogy with Jupiter (Taylor, 1966), we find that the effective equilibrium temperature is 77°K. Aumann et al. (1969) measured Saturn's effective temperature in the wavelength range from 1.5μ to 350μ to be 97±4°K. This higher value indicates an internal heat source with a total planetary output about $\left(\frac{97}{77}\right)^4 = 2.5$ times the power received from the Sun. The probable energy source is gravitational contraction (Hubbard, 1969). Low (1964) measured 93±3°K at 10μ and 95±3°K at 20μ (Low, 1966). Thus all the recent observations indicate an effective temperature near 100°K.

The results of McAdam (1969) indicate a temperature near 1700°K deep in the atmosphere or at the surface of Saturn. Such high temperatures are possible because of the large internal heat source and great optical depth of the atmosphere. If we assume the adiabatic lapse rate of 1.62°K/km used by Gulkis et al. (1969) and a cloud top temperature of 150°K, this implies an atmosphere that extends nearly 1000 km below the cloud tops! An even greater depth is implied by the lapse rate used by Wrixon and Welch (1970) in their model atmosphere. Larger values of the temperature gradient will yield more reasonable atmospheric thicknesses, but if a greater lapse rate is assumed, then a correspondingly greater fraction of ammonia must be present in order to match the high temperature observed at 73.5 cm.

APPENDIX

A. Data Analysis

1. Data Recording

The receiver output was integrated, digitized, and punched on paper tapes. The antenna servo position readings, local time, and auxiliary information were also punched on the paper tape at the beginning and end of each data set. A paper tape, representing one observing period on one source, was then converted to punched cards for analysis on a digital computer.

2. Extinction Data

A convenient model for atmospheric extinction in clear skies is given by the following equation

$$T_{OBSERVED} = T_o e^{-.23\alpha X} \qquad (A1)$$

where

$T_{OBSERVED}$ = Measured brightness temperature of an extraterrestrial source (°K)

T_o = True brightness temperature of the source (°K)

α = Zenith attenuation of the earth's atmosphere (dB)

X = Air masses along the ray path of observation

Taking the logarithm to base 10 of both sides of the equation yields

$$10 \log T_{OBSERVED} = -\alpha X + 10 \log T_o \qquad (A2)$$

Note that a plot of $10 \log T_{OBSERVED}$ versus X is a straight line with a slope of $-\alpha$ and an intercept of $10 \log T_o$. Thus by measuring $T_{OBSERVED}$

for several elevation angles, one can fit a straight line to the data and obtain the zenith attenuation α and true source temperature T_o. Figure A1 shows typical solar data taken at 3.1 mm.

The atmospheric model discussed above has two inherent weaknesses when applied to solar drift scans. The first involves the assumption that the extraterrestrial source is at a constant temperature. Rapid and sometimes dramatic enhancements of the solar flux may occur at millimeter wavelengths. Figure A2 shows data taken at 3 mm when the apparent solar temperature varied during the period of observation. The second assumption is that α is constant during the period of observation. In general, α exhibits annual and diurnal variations because of the variability of the mean atmospheric temperature and the absolute humidity. It can be shown that a linear variation of α with time will produce a parabolic rather than a linear extinction plot (Shimabukuro, 1966). The data of Fig. A3 exhibit this parabolic shape. Note that the two lines fit to the pre-transit and to the post-transit data do not have the same intercept. Thus for linearly varying extinction the model fails to predict the true source temperature. Temporal variations in α and in solar flux may produce erroneous extinction and source temperature measurements.

3. Lunar Data

Lunation data were analyzed in the same fashion as the solar extinction data. However, on those days when reliable solar extinction data were taken nearly simultaneously with the lunar observations, the

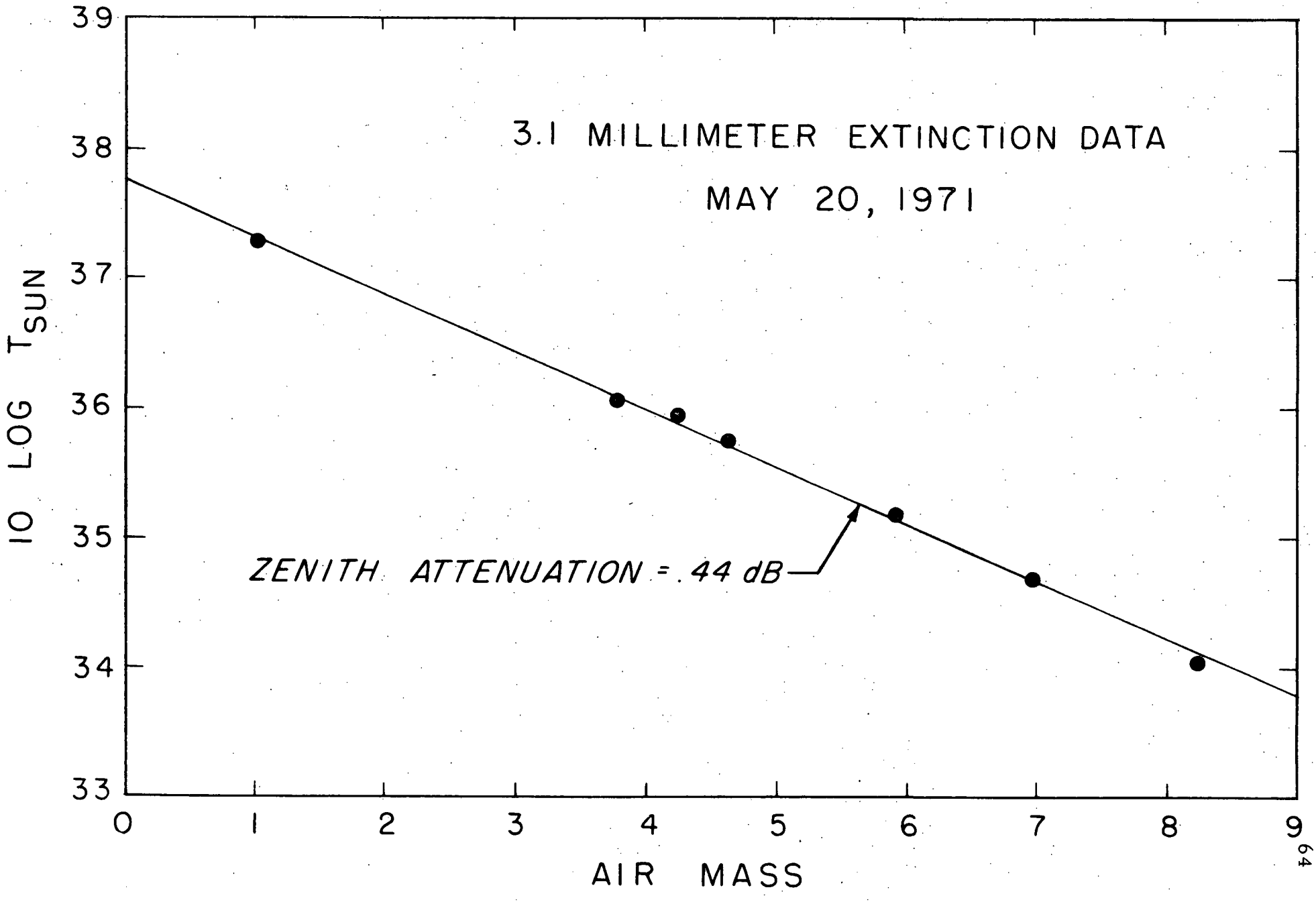
3.1 MILLIMETER EXTINCTION DATA
MAY 20, 1971
ZENITH ATTENUATION = .44 dB
10 LOG T_{SUN}
AIR MASS
39
38
37
36
35
34
33
0
1
2
3
4
5
6
7
8
9

Fig. A1

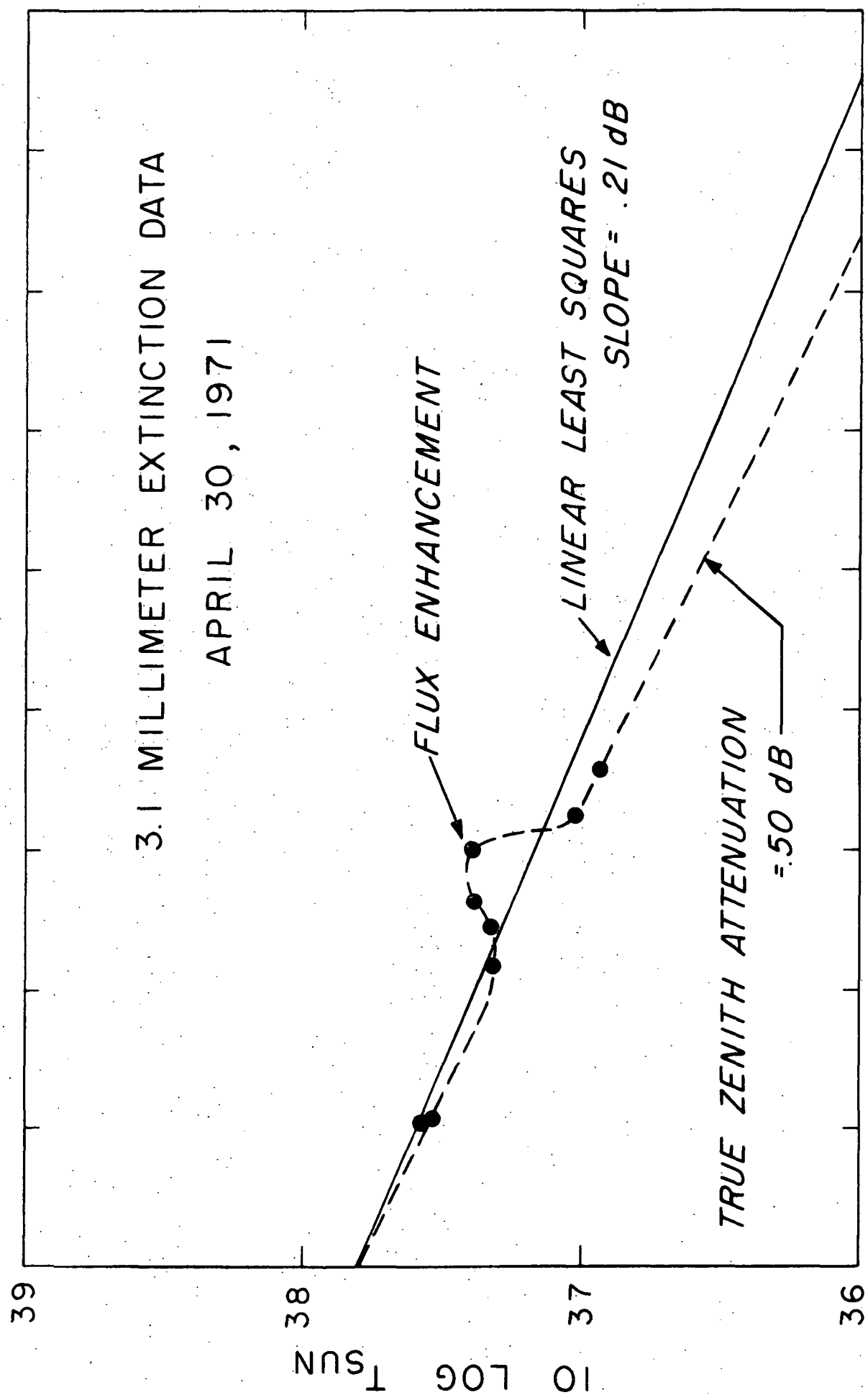
3.1 MILLIMETER EXTINCTION DATA
APRIL 30, 1971
FLUX ENHANCEMENT
LINEAR LEAST SQUARES
SLOPE = .21 dB
TRUE ZENITH ATTENUATION
=.50 dB
10 LOG T_SUN
AIR MASS
39
38
37
36
0
1
2
3
4
5
6
7
8
9

Fig. A2

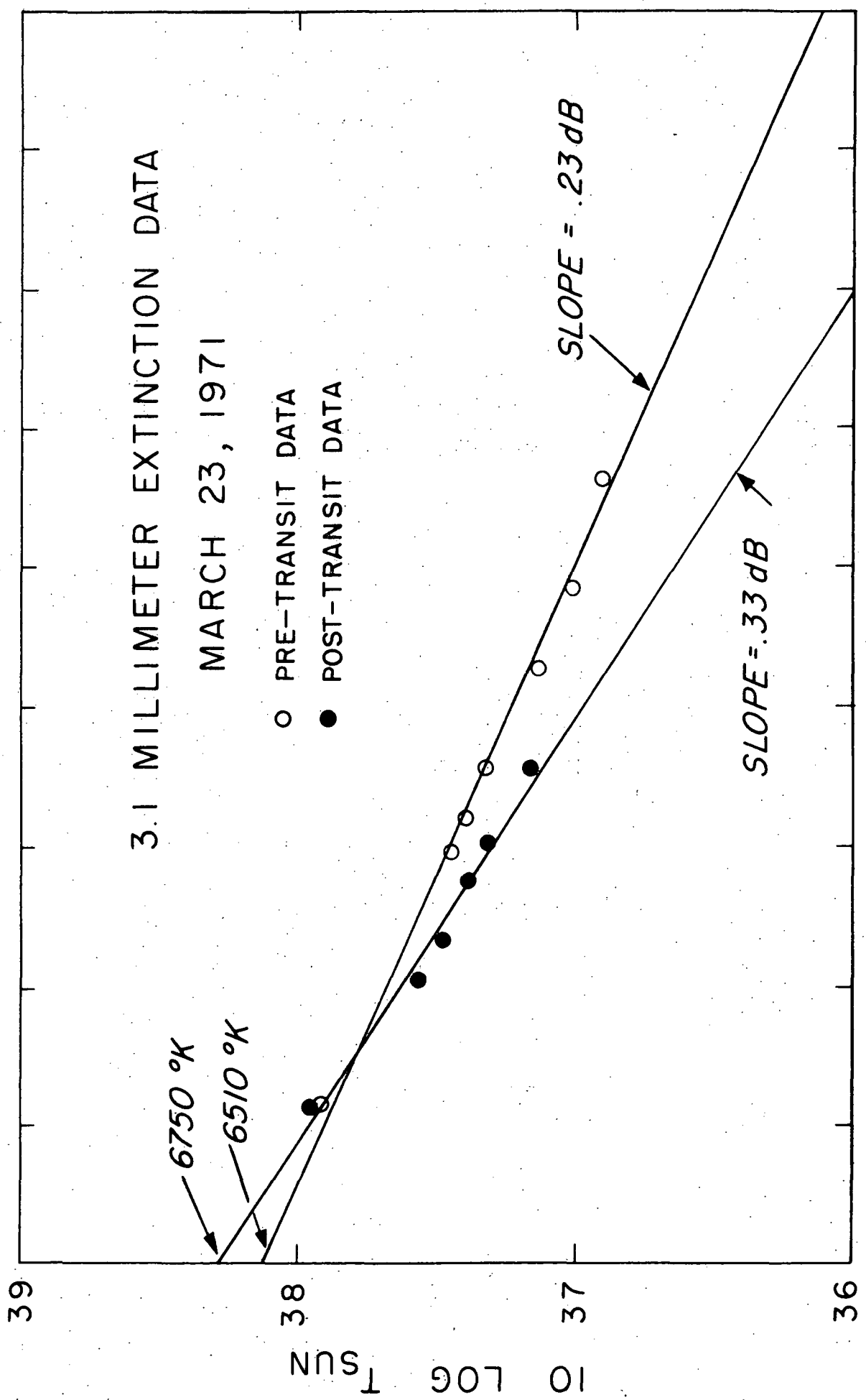
3.1 MILLIMETER EXTINCTION DATA
MARCH 23, 1971
○ PRE-TRANSIT DATA
● POST-TRANSIT DATA
SLOPE = .23 dB
SLOPE = .33 dB
6750 °K
6510 °K
10 LOG T_SUN
AIR MASS
39
38
37
36
0
1
2
3
4
5
6
7
8
9

Fig. A3

atmospheric corrections were made using the extinction derived from the solar data.

4. Planetary Data

Deflections of the output record due to planetary sources were determined by fitting lines to the baseline OFF observations and to the source ON observation. Constraining the lines to have equal slopes removes the effect of linear receiver drift. The vertical distance between the two lines is thus the deflection due to the source. Taking OFF-ON-OFF data symmetrically with equal integration time on and off the source minimizes the standard deviation of the estimate of the source deflection. Since the signal injected periodically by the noise tube has a known equivalent temperature, the source deflection can be converted to antenna temperature. Here the receiver drift was assumed to be linear with time, and the proper scale factor for a given time was found by linearly interpolating between noise tube calibrations. The correction for atmospheric extinction is

$$T_A' = T_A e^{.23\alpha X} \qquad \text{(A3)}$$

where

T_A' = Antenna temperature for a transparent atmosphere (°K)

T_A = Measured antenna temperature (°K)

For a source small compared to the half power beamwidth the disk brightness temperature is given by

$$T_B = \frac{\lambda^2 T_A'}{\Omega A_g \eta} \tag{A4}$$

where

T_B = Brightness temperature (°K)

λ = Wavelength (m)

Ω = Source solid angle (steradian)

A_g = Antenna geometrical area (m^2)

η = Antenna efficiency

The wavelength and antenna effective area are known, and the source solid angle is calculated in the ephemeris program. The antenna temperature T_A' used here is the average of the values obtained from each OFF-ON-OFF observation corrected for extinction. Thus one can calculate the effective blackbody temperature T_B.

Data were taken on Mercury, Mars, and Saturn at the calculated position only. Knowledge of the pointing error and of the shape of the main beam allows one to calculate the antenna effective area as a function of pointing error. Since Venus and Jupiter were observed over a grid of five points, these data were used to calculate the residual pointing error. A least squares fit of a two-dimensional Gaussian function representing the antenna point source response to the data was expected to yield not only the true source position but also the peak temperature. The pointing bias error was found to be 0.005° in hour angle and 0.008° in declination. Observations of seven planets in the optical guide telescope showed that the pointing error was constant for different sources

and in different regions of the sky. Later corrections in the pointing parameters reduced the residual pointing bias error to 0.001° in hour angle and 0.002° in declination. Data taken on Jupiter showed the pointing error to be constant within the accuracy of measurement over periods of several months.

The least squares fit procedure produced consistent pointing data, but the peak responses were higher than expected. Artificial data of known statistics were produced on a digital computer and subjected to this method of data analysis. It was found that the source position was correctly predicted but that the 5-point Gaussian method was a biased estimator of the peak temperature. As the signal-to-noise ratio of the data decreased, the bias was found to increase rapidly. This was also confirmed in analyzing actual planetary data. Figure A4 shows the bias as a function of signal-to-noise ratio for several different offset ratios. In the figure the offset ratio δ is defined as the ratio of the angular offset to the antenna half power half width. The signal-to-noise ratio is the peak signal power divided by the standard deviation of the noise. It is apparent, then, that the method described above could be used to determine source position, but not peak temperature unless the bias were accurately known.

A linear regression technique was developed to calculate the peak temperature if the pointing errors were known. The estimate of the peak temperature is given by

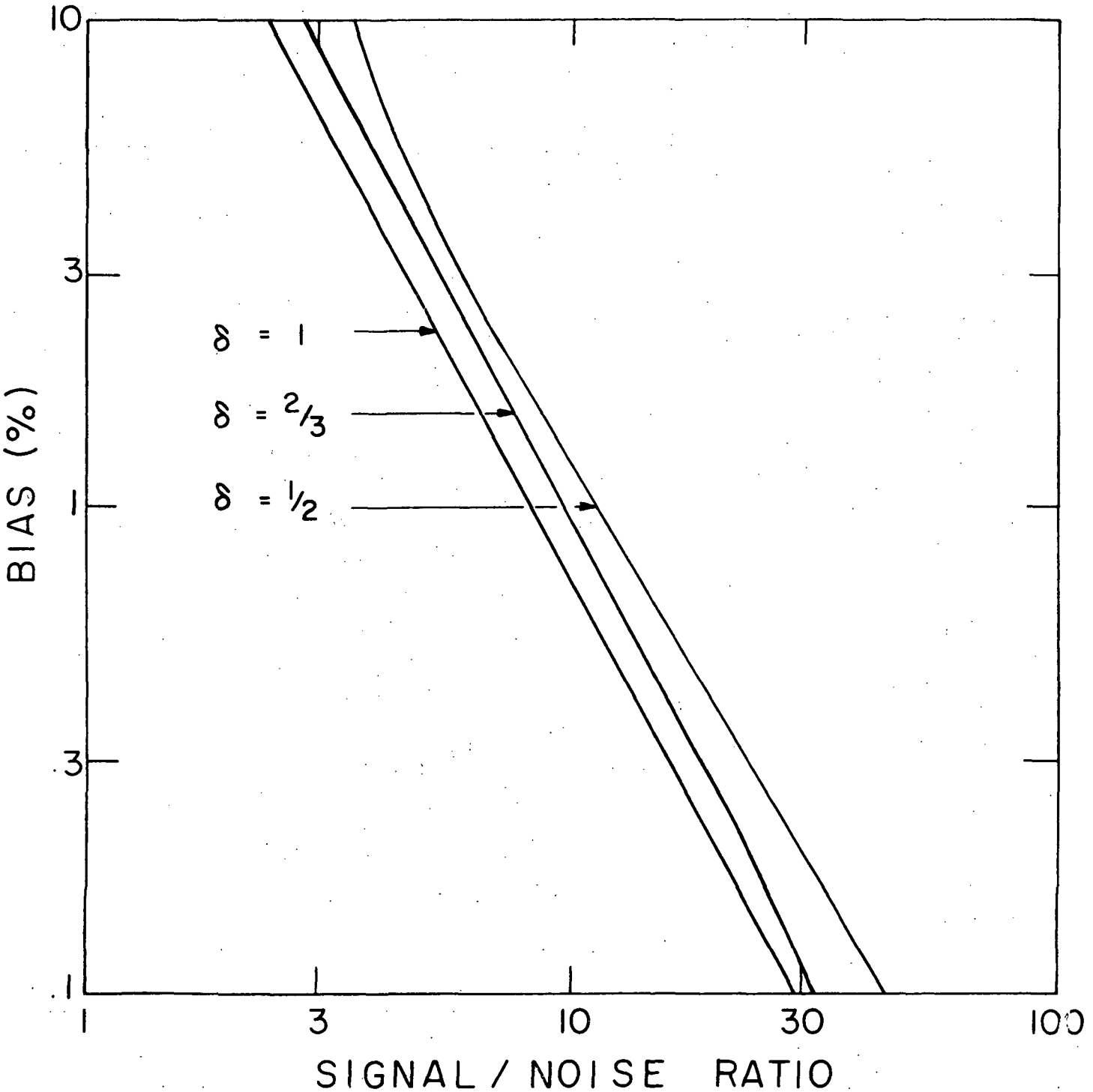

BIAS OF LEAST SQUARES FIT

Fig. A4

$$T_{EST} = \sum_{i=1}^{N} W_i T_i \tag{A5}$$

where

T_{EST} = Estimate of peak temperature (°K)

W_i = Weighting factor

T_i = Measured temperature of i^{th} point (°K)

N = Number of data points

Two constraints must be applied. First, the estimate must be unbiased. Thus

$$E[T_{EST}] = T_B \tag{A6}$$

Second, the variance of T_{EST} must be minimized. The weighting factors, found by utilizing the Lagrangian multiplier technique, are

$$W_i = \frac{\frac{g_i}{V(T_i)}}{\sum_{j=1}^{N} \frac{g_j^2}{V(T_j)}} \tag{A7}$$

where

g_i = Pointing correction factor = $\frac{A}{A_{PEAK}}$ (≤ 1.0)

$V(T_i)$ = Variance of T_i (°K)

Note that g_i is just the actual response normalized to the peak response. Also

$$V(T_{EST}) = \frac{1}{\sum_{j=1}^{N} \frac{g_j^2}{V(T_j)}} \tag{A8}$$

If the pointing correction factors and statistical properties of the data are known, this method of linear regression may be used to estimate the peak source brightness temperature.

Brightness temperatures for Mars, Jupiter, and Saturn were corrected for varying heliocentric distance by the factor $(R/R_o)^{1/2}$. R is the distance of the planet in A.U. from the Sun on the day of observation, and R_o is the mean distance of the planet from the Sun. Values of R_o adopted for Mars, Jupiter, and Saturn are 1.524, 5.203, and 9.540 A.U., respectively.

The American Ephemeris and Nautical Almanac values of 3.34", 8.41", and 4.68" were adopted for the unit semidiameters of Mercury, Venus, and Mars, respectively. However, more recent values were used for Jupiter and Saturn. Jupiter's polar and equatorial unit semidiameters were assumed to be 91.731", and 97.687", and Saturn's 73.832" and 82.728". These values are taken from Newburn and Gulkis (1971).

B. Error Analysis

1. General Considerations

One desired result of a radio astronomical measurement of the sort we are presenting in this paper is to infer the equivalent temperature of the source. In our case, this is an average temperature over the disk of a planet and is thought to be related to the physical temperature of the matter within which the radiation originates. To be scientifically

meaningful, such a "measured value," (that is, the planetary temperature) must be assigned some quantitative accuracy, i.e., error bars must be quoted. Such error bars indicate, at the very least, the opinion of the responsible party as to the accuracy of the measurement, but modern practice requires that the error bounds have a statistical meaning. That is, from the viewpoint of statistics, a measurement is but an estimate of a well defined but unknowable quantity. The estimate is apt to be somewhat different if the measurement is repeated. We model such an estimate as a random variable defined on some probabilistic experiment which could in principle be repeated a large number of times. The object of the measurement is to insure that the estimate is unbiased and of known variance, in the statistical sense. If this were true, we would have a scientifically meaningful measurement in the strictest sense.

In order to satisfy this criterion, one must either perform a number of "independent" measurements, or else set forth beyond dispute a valid statistical model for each process which contributed to the final result. For example, in the present study many factors, such as antenna gain, thermal calibrations, and atmospheric loss corrections, go into the final calculation of the planetary temperature. Errors in these quantities contribute uncertainty to the final result just as much as receiver noise or antenna tracking error. There is, however, no obvious way to design repeatable experiments to determine the statistics of these quantities: they fall outside the realm of strict probability. About all one can do is repeatedly evaluate these factors to observe the self-consistency of the

results and then subjectively estimate an overall accuracy based upon a mixture of the random and the nonrandom errors. The error, so derived, has no strict statistical meaning. It is not a standard deviation or a peak error or anything else; it is merely a subjective estimate of the overall accuracy of the quantity in question.

In the following we shall estimate errors and classify them as statistical in the strict sense or merely as a subjective estimate. The former we denote by σ and the latter by ϵ. In summary, we distinguish two types of errors: the truly random (σ) and the systematic (ϵ). We shall give the statistics of the former and estimate our overall rms accuracy of the latter. Thus we can derive an estimated accuracy for a given planetary measurement, as would be required for comparison with theory. One should bear in mind, however, that the ϵ errors are correlated for all measurements whereas the σ errors are not.

From these preliminary ideas we turn now to the discussion of the sources of error in the measurements. The estimation of the planetary temperature is a three step procedure. First we estimate the antenna temperature either with the antenna pointed nominally at the planet or nearby, as required by the five-point observing procedure described earlier; second, we take all the data from a day's observations and estimate from it what we would have measured had we pointed exactly at the planet (thus correcting for pointing error and averaging all the data together); and thirdly, the planetary temperature is derived from the estimated peak antenna temperature. We shall discuss the errors associated with each of these steps.

order to monitor receiver gain fluctuations and to calibrate the planetary signal in thermal units. The calibration scale for the observing period is determined by a linear interpolation between the individual calibrations. Sources of error are higher order receiver gain variations and receiver noise. The calibrations throughout an observation are self-consistent to about 4% peak-to-peak, and we accordingly estimate any single calibration (D_c) to be accurate to 1% (1σ).

d. The zenith atmospheric extinction - α

The atmospheric extinction is estimated through observations of sunrise or sunset, as explained earlier. The values of α at the time of observation are uncertain due to changes with time. There seems to be a diurnal variation in α in addition to the changes due to weather and seasons.

For convenience in the following discussion, let $\tau = .23\alpha$. Now τ is the zenith optical depth in nepers. If we model τ as a Gaussian random variable having a mean $\bar{\tau}$ and standard deviation σ, we find that the factor $e^{\tau X}$ has the following properties

$$E\left[e^{\tau X}\right] = e^{\bar{\tau}X}\left[e^{\frac{\sigma^2 X^2}{2}}\ \frac{1 + \mathrm{Erf}\left(\frac{\bar{\tau}}{\sigma} + \sigma X\right)}{1 + \mathrm{Erf}\left(\frac{\bar{\tau}}{\sigma}\right)}\right] \qquad (A11)$$

and

$$E\left[\left(e^{\tau X} - e^{\bar{\tau}X}\right)^2\right] = \sigma(X) \qquad (A12)$$

2. Antenna Temperature

The antenna temperature during an observation of some point on the sky (relative to the planet) is estimated by the formula

$$T_i(\underline{X}_i) = \frac{T_c D_i}{D_c} e^{.23\alpha X} \qquad \text{(A9)}$$

where

$T_i(\underline{X}_i)$ = Antenna temperature at position $\underline{X}_i$ relative to the planet

D_i = Receiver output deflection due to planet

T_c = Equivalent temperature of calibration signal (°K)

D_c = Receiver output deflection due to calibration signal

α = Zenith atmospheric extinction in dB at the time of observation

X = Air masses along the ray path of observation

a. Receiver output deflection due to planetary signal - D_i

In a sensitivity limited measurement the receiver noise is the limiting factor. This shows up in the uncertainty of the output deflection due to the planet. The statistics of D_i are well behaved and well understood, and depend on the receiver sensitivity and the integration time on the source. In thermal units

$$\sigma_i = \sqrt{2}\,\frac{\Delta T_{rms}}{\sqrt{t}} \qquad \text{(A10)}$$

where

σ_i = Standard deviation of T_i due to uncertainty in D_i (°K)

t = Integration time in seconds

ΔT_{rms} = Receiver sensitivity with $t = 1$ sec

In the observations ΔT_{rms} is evaluated by examining the statistics of the baseline. The individual σ_i's are computed and retained for weighting in the next operation.

b. The calibration signal equivalent temperature - T_c

The evaluation of the calibration signal is discussed earlier in this paper. Sources of systematic error are termination VSWR corrections, incomplete thermal coupling between the water bath and termination, thermometer inaccuracy, drift during calibration, and changes in noise tube properties with time. Random errors enter through the receiver noise.

The calibration data at 3.1 mm are presented in Table II. We note no change in time and the scatter is larger than expected from receiver noise alone. We attribute this to a combination of the errors cited above, and from the internal scatter of the data we calculate a 1.6% random error. To correct for termination VSWR and waveguide loss, we reduce the average by 1.0% and add 1.0% uncertainty. Hence at 97 GHz the calibration signal is 80.6°K±1.6% (1σ)±1.0% (1ϵ). In the absence of repeated calibrations at 35 GHz, we will assume the same relative accuracies as a conservative measure.

c. Receiver output deflection due to calibration signal - D_c

During the course of observations the calibration signal is injected into the receiver at intervals of approximately 20 minutes in

where

$\sigma = \sqrt{V(\tau)}$, the standard deviation of the estimate of the zenith optical depth.

Thus there is some possibility of bias due to uncertainty of τ, but the corrections are quite small for reasonable values of $\bar{\tau}$ and σ. For σ = .10 dB, a conservative estimate in the uncertainty of opacity, the relative uncertainty in the atmospheric correction is nominally 2% at 3.1 mm and 1% at 8.6 mm. These errors are consistent with the internal scatter of the solar data in Fig. 3 and 4.

3. Peak Antenna Temperature

Once the individual antenna temperatures of the planet are determined, the peak antenna temperature Ta_e is given by the linear estimator

$$Ta_e = \frac{\sum_{i=1}^{N} \frac{g(\underline{X}_i)}{\sigma_i^2} T_i}{\sum_{i=1}^{N} \frac{g^2(\underline{X}_i)}{\sigma_i^2}} \qquad \text{(A13)}$$

where $g(\underline{X}_i)$ is the expected response at $\underline{X}_i$ of the planet normalized to the peak response (essentially the point source response of the antenna).

We consider the effects of pointing errors on the averaging by approximating the beam as Gaussian and letting pointing errors contain bias and random errors. Assuming the pointing errors are uncorrelated in the 1, 2 directions (hour angle, declination) with standard deviations

ϵ_1 and ϵ_2, and biased by angles δ_1 and δ_2, respectively, we find, approximating a sum by an integral,

$$E[Ta_e] \approx Ta \frac{e^{-\frac{1}{2}\frac{\delta_1^2 + \delta_2^2}{\theta^2} \ell n\, 2}}{\sqrt{\left[1 + \ell n\, 2\left(\frac{\epsilon_1}{\theta}\right)^2\right]\left[1 + \ell n\, 2\left(\frac{\epsilon_2}{\theta}\right)^2\right]}} \quad \text{(A14)}$$

and

$$E[(Ta_e - Ta)^2] = \sum_{i=1}^{N} \frac{g^2(\underline{X}_i)}{\sigma_i^2} \quad \text{(A15)}$$

where θ = 1/2 the half power beamwidth.

Thus we see that random and bias pointing errors introduce a bias in determining Ta_e. For the 3.1 mm observations, we estimate $\delta_1 = \delta_2 = \frac{\theta}{10}$ and $\epsilon_1 = 0$, $\epsilon_2 = \frac{\theta}{10}$ as a worst case. In this case the bias is about 1.5% low. Since this bias is down and the bias in extinction corrections is up and of approximately the same value, we shall make no correction for the two biases, but increase the overall uncertainty slightly to account for their combined effects.

In Section IV the receiver noise is tabulated separately for each measurement since it is the major noise component. These errors are σ-type errors.

4. Brightness Temperature

The final step in the data reduction is the inference of the planetary temperature from the antenna temperature. This is done through the expression

$$T_B = \frac{\lambda^2 \Omega \, Ta_e \, F_B}{A_g \eta} \qquad \text{(A16)}$$

where

T_B = Disk brightness temperature of the planet (°K)

λ = Wavelength of observation (m)

A_g = Antenna geometrical area (m^2)

η = Antenna efficiency

Ω = Solid angle subtended by the planetary disk (steradian)

Ta_e = Peak antenna temperature corrected for extinction (°K)

F_B = A beam broadening factor to account for the finite size of source with respect to the beam (Cogdell, 1969b)

In the above equation we immediately dismiss λ, Ω, and F_B as sources of significant uncertainty. Ta_e has been discussed in the previous section.

The major source of error in absolute measurements is usually in the antenna gain or efficiency. In the present case the gain values are scaled between a measured value at a higher frequency and a calculated theoretical efficiency. This theory has been developed by Davis and Cogdell (1971) and will not be discussed here.

The measured value of the gain is based upon the calculated gain of a conical horn, a difference in gain measured by an IF (cuttoff mode) attenuator, and some routine waveguide loss measurements which were made using radiometric technique. The calculated gain is based upon well established diffraction theory, corroborated by comparing measured patterns of the antenna with theoretical patterns calculated on the

basis of the same theory. The measured patterns are more sensitive to error and approximation than the gain calculations. Sources of errors in each component have been carefully estimated. The scaling theory offers some reduction of the error bounds. The relative accuracies are 5.3% at 97.1 GHz and 1.4% at 35.0 GHz. These errors are of the systematic or ε-type.

5. Summary

We now will consider the various errors, except for the receiver noise, which varies from measurement to measurement. The remainder are estimated errors and are the same for all measurements. They are summarized in Table AI. The overall errors are Pythagorean sums, as is customary thought not indisputably justifiable.

TABLE AI

ERROR SUMMARY

Source	Estimated bias (%)		Estimated ε(%)		Estimated σ(%)	
	35 GHz	97 GHz	35 GHz	97 GHz	35 GHz	97 GHz
D_i	0	0	0	0	---	---
T_c	-1.0	-1.0	1.0	1.0	2.4	2.4
τ	1.0	1.0	0	0	2.0	1.0
Pointing	- .7	- .3	0	0	.7	.3
Tracking	- .7	- .3	0	0	.7	.3
η	0	0	5.3	1.4	0	0
Overall	-1.4%	- .6%	5.4%	1.7%	3.3%	2.7%

REFERENCES

AUMANN, H. H., GILLESPIE, C. M., JR., AND LOW, F. J. (1969). The internal powers and effective temperatures of Jupiter and Saturn. Astroph. J. 157, L69-L72.

BERGE, G. L. (1968). Recent observations of Saturn, Uranus, and Neptune at 3.12 cm. Astroph. Lett. 2, 127-131.

BERGE, G. L., AND READ, R. B. (1968). The microwave emission of Saturn. Astroph. J. 152, 755-764.

BRAUN, L.D., AND YEN, J. L. (1968). Some radio observations at 35 GHz (abstract). Astron. J. 73, S168.

CLARDY, D. E., AND STRAITON, A. W. (1968). Radiometric measurements of the Moon at 8.6 mm and 3.2 mm. Astrophy. J. 154, 775-782.

COGDELL, J. R. (1969a). Calibration program for the 16-foot antenna. The University of Texas at Austin, Millimeter Wave Sciences Tech. Report No. NGL-006-69-1.

COGDELL, J. R. (1969b). The use of gaussian functions in radio astronomy source measurements. The University of Texas at Austin, Electrical Engineering Research Laboratory Tech. Memo. No. NGL-006-69-2.

COGDELL, J. R., McCUE, J. J., KALACHEV, P. D., SALOMONOVICH, A. E., MOISEEV, I. G., STACEY, J. M., EPSTEIN, E. E., ALTSHULER, E. E., FEIX, G., DAY, J. W., HVATUM, H., WELCH, W. J., AND BARATH, F. T. (1970). High resolution millimeter reflector antennas. IEEE Trans. Antennas Propagation AP-18, 515-529.

COGDELL, J. R. (1972). Pencil beam observation of a large microwave outburst at 94.8 GHz. Solar Physics (in press).

COGDELL, J. R., AND DAVIS, J. H. (1972). Random and systematic phase errors in reflector antennas. (unpublished paper).

COOK, J. J., CROSS, L. G., BAIR, M. E., AND ARNOLD, C. B. (1960). Radio detection of the planet Saturn. Nature 188, 393-394.

DAVIES, R. D., AND WILLIAMS, D. (1966). Observations of the continuum emission from Venus, Mars, Jupiter, and Saturn at 21.2 cm wavelength. Planet. Space Sci. 14, 15-32.

DAVIES, R. D., BEARD, M., AND COOPER, B. F. (1964). Observations of Saturn at 11.3 centimeters. Phys. Res. Lett. 13, 325-327.

DAVIS, J. H., AND COGDELL, J. R. (1969). Pointing of the 16-foot antenna. The University of Texas at Austin, Electrical Engineering Research Laboratory Tech. Memo. No. NGL-006-69-3.

DAVIS, J. H. (1970). The evaluation of reflector antennas. The University of Texas at Austin, Electrical Engineering Research Laboratory Tech. Report No. NGL-006-70-1.

DAVIS, J. H., AND COGDELL, J. R. (1970). Astronomical refraction at millimeter wavelengths. IEEE Trans. Antennas Propagation AP-18, 490-493.

DAVIS, J. H., AND COGDELL, J. R. (1971). Reflector efficiency evaluation by frequency scaling. IEEE Trans. Antennas Propagation AP-19, 58-63.

DENT, W. A., KLEIN, M. J., AND ALLER, H. D. (1965). Measurements of Mars at λ3.75 cm from February to June, 1965. Astrophy. J. 142, 1685-1688.

DICKEL, W., WARNOCK, W., AND MEDD, W. J. (1968). Lack of phase variation of Venus. Nature 220, 1183-1185.

DICKEL, J. R., DEGIOANNI, J. J., AND GOODMAN, G. C. (1970). The microwave spectrum of Jupiter. Radio Sci. 5, 517-527.

DRAKE, F. D. (1962). Microwave spectrum of Saturn. Nature 195, 893-894.

EFANOV, V. A., KISLYAKOV, A. G., MOISEEV, I. G., AND NAUMOV, A. I. (1969). Radio emission of Venus and Jupiter at 2.25 and 8 mm. Soviet Ast.-AJ. 13, 110-113.

EFANOV, V. A., MOISEEV, I. G., KISLYAKOV, A. G., AND NAUMOV, A. I. (1971). Mars and Jupiter: radio emission at 2.3 mm and 8.15 mm. Icarus 14, 198-203.

EPSTEIN, E. E. (1965). 3.3-mm observations of Venus in 1964. Astror. J. 70, 721-725.

EPSTEIN, E. E. (1968). Mars, Jupiter, and Saturn: 3.4 mm brightness temperatures. Astrophy. J. 151, L149-L152.

EPSTEIN, E. E., OLIVER, J. P., SOTER, S. L., SCHORN, R. A., AND WILSON, W. J. (1968). Venus: on an inverse variation with phase in the 3.4-mm emission during 1965 through 1967. Astron. J. 73, 271-274.

EPSTEIN, E. E., DWORETSKY, M. M., FOGARTY, W. G., MONTGOMERY, J. W., AND COOLEY, R. C. (1970a). Mercury: epilith physical parameters and a hermocentric longitude dependence of its 3.3-mm radiation. Radio Sci. 5, 401-409.

EPSTEIN, E. E., DWORETSKY, M. M., MONTGOMERY, J. W. AND FOGARY, W. G. (1970b). Mars, Jupiter, Saturn, and Uranus: 3.3 mm brightness temperatures and a search for variations with time or phase angle. Icarus 13, 276-281.

EPSTEIN, E. E. (1971). Mars: a possible discrepancy between the radio spectrum and elementary theory. Icarus 14, 214-221.

EVANS, J. V., AND HAGFORS, T. (1968). Radar Astronomy, McGraw-Hill, New York.

FIELD, G. B. (1959). The source of radiation from Jupiter at decimeter wavelengths. J. Geoph. Res. 64, 1169-1177.

FOUNTAIN, J. A., AND WEST, E. A. (1970). Thermal conductivity of particulate basalt as a function of density in simulated lunar and Martian environments. J. Geophys. Res. 75, 4063-4069.

FRENKEL, L., AND WOODS, D. (1966). Microwave absorption in compressed CO_2. J. Chem. Phys. 44, 2219.

GIORDMAINE, J. A., ALSOP, L. E., TOWNES, C. H., AND MAYER, C. H. (1959). Observations of Jupiter and Mars at 3 cm wavelength (abstract). Astron. J. 64, 332.

GOLOVKOV, V. K., AND LOSOVSKII, B. YA. (1968). Measurements of the phase dependence of the 0.8-cm radio emission of Mercury, and some properties of its surface layer. Soviet Astron.-AJ 12, 229-302.

GULKIS, S., McDONOUGH, T. R., AND CRAFT, H. (1969). The microwave spectrum of Saturn. Icarus 10, 421-427.

HO, W., KAUFMANN, I. A., AND THADDEUS, P. (1966). Laboratory measurement of microwave absorption in models of the atmosphere of Venus. J. of Geophys. Res. 71, 5091-5108.

HOBBS, R. W., McCULLOUGH, T. P., AND WAAK, J. A. (1968). Measurements of Mars at 1.55-cm and 0.95-cm wavelengths. Icarus 9, 360-363.

HOBBS, R. W., AND KNAPP, S. L. (1971). Planetary temperatures at 9.55 mm wavelength. Icarus 14, 204-209.

HUBBARD, W. B. (1969). Thermal models of Jupiter and Saturn. Astron. J. 155, 333-344.

HUBBARD, W. B., NATHER, R. E., EVANS, D. S., TULL, R. G., WELLS, D. C., VAN CITTERS, G. W., WARNER, B., AND VANDEN BOUT, P. (1972). The occultation of Beta Scorpii by Jupiter and I_o - I. Jupiter. Astron. J. (in press).

HUGHES, M. P. (1966). Planetary observations at a wavelength of 6 cm. Planet. Space Sci. 14, 1017-1022.

INGERSOLL, A. P. (1971). Mars: occurrence of liquid water. Planetary Atmospheres (Sagan et al., eds.), 247-250.

KAFTAN-KASSIM, M. A., AND KELLERMANN, K. I. (1967). Measurements of the 1.9-cm thermal radio emission from Mercury. Nature 213, 272-273.

KALAGHAN, P. M., AND WULFSBERG, K. N. (1968). Radiometric observations of the planets Jupiter, Venus, and Mars at a wavelength of 8.6 mm. Astrophys. J. 154, 771-773.

KALAGHAN, P. M., WULFSBERG, K. N., AND TELFORD, L. E., (1968). Observations of the phase effect of Venus at 8.6-mm wavelength. Astron. J. 73, 969-971.

KALAGHAN, P. M., AND TELFORD, L. E. (1971). Radio observations of Mars at 8.57 millimeters. Astrophys. J. 170, L77-L79.

KELLERMANN, K. I. (1965). Radio observations of Mars. Nature 206, 1034-1035.

KELLERMANN, K. I., AND PAULINY-TOTH, I. I. K. (1966). Observations of the radio emission of Uranus, Neptune, and other planets at 1.9 cm. Astrophys. J. 145, 954-957.

KELLERMANN, K. I. (1966). The thermal radio emission from Mercury, Venus, Mars, Saturn, and Uranus. Icarus 5, 478-490.

KELLERMANN, K. I. (1970). Thermal radio emission from the major planets. Radio Sci. 5, 487-493.

KISLYAKOV, A. G., KUZMIN, A. D., AND SALOMONOVICH, A. E. (1962). 4-mm radio emission from Venus. Soviet Astron.-AJ 6, 328-332.

KISLYAKOV, A. G., AND LEBSKII, YU. V. (1968). Radio emission of the Crab Nebula and Jupiter at 77.5-GHz frequency. Soviet Astron.-AJ 14, 561-564.

KLEIN, M. J. (1968). The planet Mercury: measurements of variations in the microwave disk temperature. Thesis, The University of Michigan, Ann Arbor, Michigan.

KLEIN, M. J. (1970). Mercury: recent observations at 3.75-cm wavelength-summary. Radio Sci. 5, 397-400.

KLEIN, M. J. (1971). Mars: measurements of its brightness temperature at 1.85 and 3.75 cm wavelength. Icarus 14, 210-213.

KOSTENKO, V. I., PAVLOV, A. V., SHOLOMITSKY, G. B., SLYSH, V. I., SOGLASNOVA, V. A. AND ZABOLOTNY, V. F (1970). The brightness temperatures of planets in the wavelength range centered at 1.4 mm. Paper and preprint presented at the XIV General Assembly of the International Astronomical Union, 18-27 August, Brighton, England.

KUZMIN, A. D., LOSOVSKY, B. YA., AND VETUKHNOVSKAYA, YU. N. (1971). Measurements of Mars radio emission at 8.22 mm and evaluation of thermal and electrical properties of its surface. Icarus 14, 192-195.

KROTIKOV, V. D., AND TROITSKII, V. S. (1964). Radio emission and the nature of the Moon. Soviet Phys. 6, 841-871.

LAW, S. E., AND STAELIN, D. H. (1968). Measurements of Venus and Jupiter near 1-cm wavelength. Astrophys. J. 154, 1077-1086.

LOW, F. J. (1964). Infrared brightness temperature of Saturn. Astron. J. 69, 550.

LOW, F. J., AND DAVIDSON, A. W. (1965). Lunar observations at a wavelength of 1 millimeter. Astrophy. J. 142, 1278-1282.

LOW, F. J. (1966). Observations of Venus, Jupiter, and Saturn at $\lambda 20\mu$. Astron. J. 71, 391.

McADAM, W. B. (1969). Observations of emission from Saturn at 408 MHz. Proc. Astron. Soc. Australia 1, 199-201.

MAYER, C. H., AND McCULLOUGH, T. P. (1971). Microwave radiation of Uranus and Neptune. Icarus 14, 187-191.

MENZEL, D. H., COBLENTZ, W. W., AND LAMPLAND, C. O. (1926). Planetary temperatures derived from water-cell transmission. Astrophys. J. 63, 177-187.

MOROZ, V. I., DAVYDOV, V. D., AND ZHEGULEV, V. S. (1969). Photometric and spectroscopic observations of planets in the 8-14μ range. Astron. Zh. 46, 136-146.

MORRISON, D. (1969a). Thermal models and microwave temperatures of the planet Mercury. Smithsonian Astrophys. Obs., Spec. Rpt. 292.

MORRISON, D. (1969b). Venus: absence of a phase effect at 2-cm wavelength. Science 163, 815-816.

MORRISON, D., SAGAN, C., AND POLLACK, J. B. (1969). Martian temperatures and thermal properties. Icarus 11, 36-45.

MORRISON, D., AND KLEIN, M. J. (1970). The microwave spectrum of Mercury. Astrophys. J. 160, 325-332.

MUHLEMAN, D. O., AND SATO, T. (1965). Observations of Mars at 12.5-cm wavelength. Radio Sci. 69D, 1580.

MUHLEMAN, D. O. (1969). Microwave opacity of the Venus atmosphere. Astron. J. 74, 57-69.

MURRAY, B. C. (1967). Infrared radiation from the daytime and nighttime surfaces of Mercury (abstract). Trans. Amer. Geophys. Union 48, 148.

NEUGEBAUER, G., MUNCH, G., KIEFFER, H., CHASE, S. C., JR., AND MINER, E. (1971). Mariner 1969 infrared radiometry results: temperatures and thermal properties of the Martian surface. Astron. J. 76, 719-728.

NEWBURN, R. L., JR., AND GULKIS, S. (1971). A brief survey of the outer planets Jupiter, Saturn, Uranus, Neptune, Pluto, and their satellites, Jet Propulsion Laboratory Tech. Report 32-1529.

PAULINY-TOTH, I. K., AND KELLERMANN, K. I. (1970). Millimeter-wavelength measurements of Uranus and Neptune. Astrophys. Lett. 6, 185-187.

PETIT, E., AND NICHOLSON, S. B., (1924). Radiation measures on the planet Mars. Publ. Astron. Soc. Pacific 36, 269-272.

POLLACK, J. B., AND MORRISON, D. (1970). Venus: determination of atmospheric parameters from the microwave spectrum. Icarus 12, 376-390.

POLLACK, J. B., AND SAGAN, C. (1970). Studies of Mars (very early in the era of spacecraft reconnaissance). Radio Sci. 5, 443-464.

POLLACK, J. B., AND MORRISON, D. (1971). Venus: determination of atmospheric parameters from the microwave spectrum. Planetary Atmospheres (Sagan et al., eds.) 28-31.

REBER, E. E. (1970). Brightness temperatures of the quiet Sun and the new Moon at 3.3- and 5.7-mm wavelengths. Icarus 12, 348-359.

ROSE, W. K., BOLOGNA, J. M., AND SLOANAKER, R. M. (1963). Linear polarization of the 3200-Mc/sec radiation from Saturn. Phys. Rev. Lett. 10, 123-125.

RUZE, J. (1966). Antenna tolerance theory - a review. Proc. IEEE 54, 633-640.

SAGAN, C. (1971). The trouble with Venus. Planetary Atmospheres (Sagan et al. eds.), 116-128.

SAGAN, C., AND VEVERKA, J. (1971). The microwave spectrum of Mars: an analysis. Icarus 14, 222-234.

SALOMONOVICH, A. E. (1965). The observations of radio emission from the planets Mercury, Mars, and Saturn at wavelength of 8 mm. Radio Sci. 69D, 1576.

SELING, T. V. (1970). Observations of Saturn at λ 3.75 cm. Astron J. 75, 67-68.

SHIMABUKURO, F. I. (1966). Propagation through the atmosphere at a wavelength of 3.3 mm. IEEE Trans. Antennas Propagation AP-14, 228-235.

SHIMABUKURO, F. I., AND STACEY, J. M. (1968). Brightness temperature of the quiet Sun at centimeter and millimeter wavelengths. Astrophys. J. 152, 777-782.

SINCLAIR, A. C. E., BASART, J. P., BUHL, D., GALE, W. A. AND LEWABITY, M. (1970). Preliminary results of interferometric observations of Venus at 11.1-cm wavelength. Radio Sci. 5, 347-354.

SINTON, W. M. (1964). Physical researches on the brighter planets. AFCRL-64-926, Air Force Cambridge Research Laboratories, Bedford, Massachusetts.

SPENCER, R. C. (1949). A least square analysis of the effect of phase errors on antenna gain. Air Force Cambridge Research Center Report E5025.

SOTER, S. L. (1966). Mercury: infrared evidence for nonsynchronous rotation. Science 153, 1112-1113.

STANKEVICH, K. S. (1970). Observations of Mars and Venus at 11.1 cm. Austral. J. Phys. 23, 111-112.

TAKAHASHI, K. (1967). An investigation of solar emission at frequencies of 35 Gc, 70 Gc, and 94 Gc with a 4.88 meter diameter telescope. Astrophys. J. 148, 497-500.

TAYLOR, D. J. (1966). Spectrophotometry of Jupiter's 3400-10000 Å spectrum and a bolometric albedo for Jupiter. Icarus 4, 362-373.

TOLBERT, C. W., AND STRAITON, A. W. (1964). An investigation of 35 Gc/s, 70 Gc/s and 94 Gc/s Cytherean radiation. Nature 204, 1242-1245.

TOLBERT, C. W. (1965). Millimeter wavelength spectra of the Crab and Orion Nebulae. Nature 206, 1304-1307.

TOLBERT, C. W., AND STRAITON, A. W. (1965). An investigation of Tau A and Sgr A millimeter wavelength radiation. Astron. J. 70, 177-180.

TOLBERT, C. W., STRAITON, A. W., AND KRAUSE, L. C. (1965). A 16-foot millimeter wavelength antenna system, its characteristics and its applications. IEEE Trans. Antennas Propagation AP-13, 225-229.

TOLBERT, C. W. (1966). Observed millimeter brightness temperatures of Mars, Jupiter, and Saturn. Astron. J. 71, 30-32.

TRAFTON, L. M. (1967). Model atmospheres of the major planets. Astroph. J. 147, 765-781.

TRAFTON, L. M. (1972). Private communication.

TROITSKII, V. S. (1967). Investigation of the surfaces of the Moon and planets by means of thermal radiation. Proc. Roy. Soc. (London) A296, 366-398.

TROITSKII, V. S. (1970). On the possibility of determining the nature of the surface material of Mars from its radio emission. Radio Sci. 5, 481-486.

ULICH, B. L. (1972). Observations of the total lunar eclipse on February 10, 1971 at 3.1 mm wavelength. Icarus (in press).

WELCH, W. J., AND THORNTON, D. D. (1965). Recent planetary observations at wavelengths near 1 cm (abstract). Astron J. 70, 149.

WELCH, W. J., THORNTON, D. D., AND LOHMAN, R. (1966). Observations of Jupiter, Saturn, and Mercury at 1.53 centimeters. Astrophys. J. 146, 799-809.

WRIXON, G. T., AND WELCH, W. J. (1970). The millimeter wave spectrum of Saturn. Icarus 13, 163-172.

WRIXON, G. T., WELCH, W. J., AND THORNTON, D. D. (1971). The spectrum of Jupiter at millimeter wavelengths. Astrophys. J. 169, 171-183.

YERBURY, M.J., CONDON, J. J., JAUNCEY, D. L., AND GULKIS, S. (1971). Observations of Saturn at a wavelength of 49.5 cm. Submitted to Bull. American Astron. Soc.